Master thesis

Evaluation of Background Light Suppression Characteristic and Range Finding Accuracy for 3-D Measurement using Smart Image Sensor

スマートイメージセンサーを用いた形状計測における背景光抑圧特性及び測距精度の評価

Xinghua Hu

Student ID: 37-106518

Supervisor: Professor Makoto Ikeda

Dept. of Electrical Engineering

The University of Tokyo

08 February, 2012 Submitted

Contents

List of Figures

List of Tables

Chapter 1

Introduction

1.1 Background

Since we are living in a three-dimensional world, an adequate description of our environment for many applications includes the relative position and motion of the different objects in a scene. Nature has satisfied this need for spatial perception by providing most animals with at least two eyes. This stereo vision ability is the basis that allows the brain to calculate qualitative depth information of the observed scene. Imaging 3-D measurement with useful distance resolution has mainly been realized with several methodologies. These methodologies can be categorized into three classifications. As shown in Fig. 1.1, these classifications include:

Triangulation

The triangulation method can be also divided into passive triangulation and active triangulation by the principles. The typical passive method is called stereo-matching [1]-[9]. As shown in Fig. 1.2(a), the stereo-matching system using two or more cameras from different angles, to acquire range maps by matching the patterns of the images in each camera. Although stereo-matching system can be realized by a simple system configuration, it need to suffer the huge computational complexity. The passive methods cannot calculate the distance of objects that is hard to be distinguished, such as white plane or unclear object. light-section method, which is also called active triangulation method, has a capability of high range accuracy, and it is efficient for high-quality range map capture in a middle-range target scene. The principle of range calculation is same as the stereo-matching from the point of triangulation.

A light-section range-finding system consists of a sheet beam projector and a position sensor as shown in Fig. 1.2(b). The light-section range finding method realizes high-accuracy range map capture because of active light projections, however, many frames are necessary for the position detection during the beam scanning in order to acquire a range map. It is difficult for a standard image sensor to attain a high frame rate. So, by replacing the sheet beam projector, 2-D structured light illumination and 2-D imaging to perform 3-D triangulation measurements without scanning are used for further advanced technique, but it needs much computation to specify 2-D image the as well as stereo-matching method.

Time-of-Flight(TOF)

The TOF[10]-[17] method, as shown in Fig. 1.2(c), a projected light is reflected from a target object with some delay in proportion to the distance as shown in Fig. 1.2(c). The arrival time of the reflected light is acquired by a special photo detector. The range resolution is basically determined by the time resolution independently of a target distance, therefore the TOF is suitable for a long-distance range-finding. Range accuracy is, however, limited at a couple of centimeters by a electronic shutter speed of a special photo detector.

Interferometry

The interferometry[18]-[24] method, as shown in Fig. 1.2(d), which is well-known for the Michelson interferometer, can be equivalently interpreted as a TOF principle, since the run-time difference between the reference and measurement path is evaluated. By employing multi-wave interferometry, where two very closely spaced wavelengths are used at the same time, this method enable absolute measurements over several tens of centimeters. However, a distance range is from micrometers to several centimeters to realize highly accurate measurement.

Fig. 1.3 shows a comparison in terms of distance and resolution. After we have read the introduction before, we have know the concepts and principles of triangulation, time-of-flight and interferometry. Although these concepts and principles seems simple, actually it is still hard for us to find a method totally satisfied our needs. Our system always have to work in variable environments, some of these environments are commonly extremely hardness ,such as some systems have to work in the sunlight, some have to work in variable weather condi-

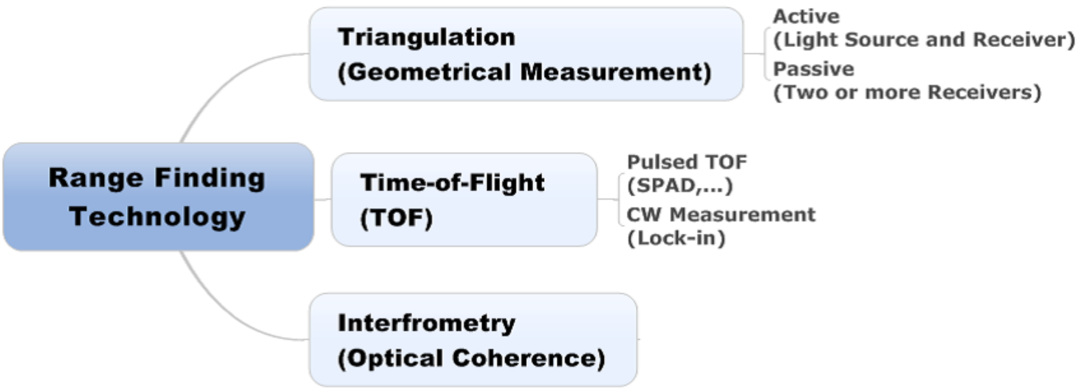

Figure 1.1 Classification of 3-D Measurement Technology

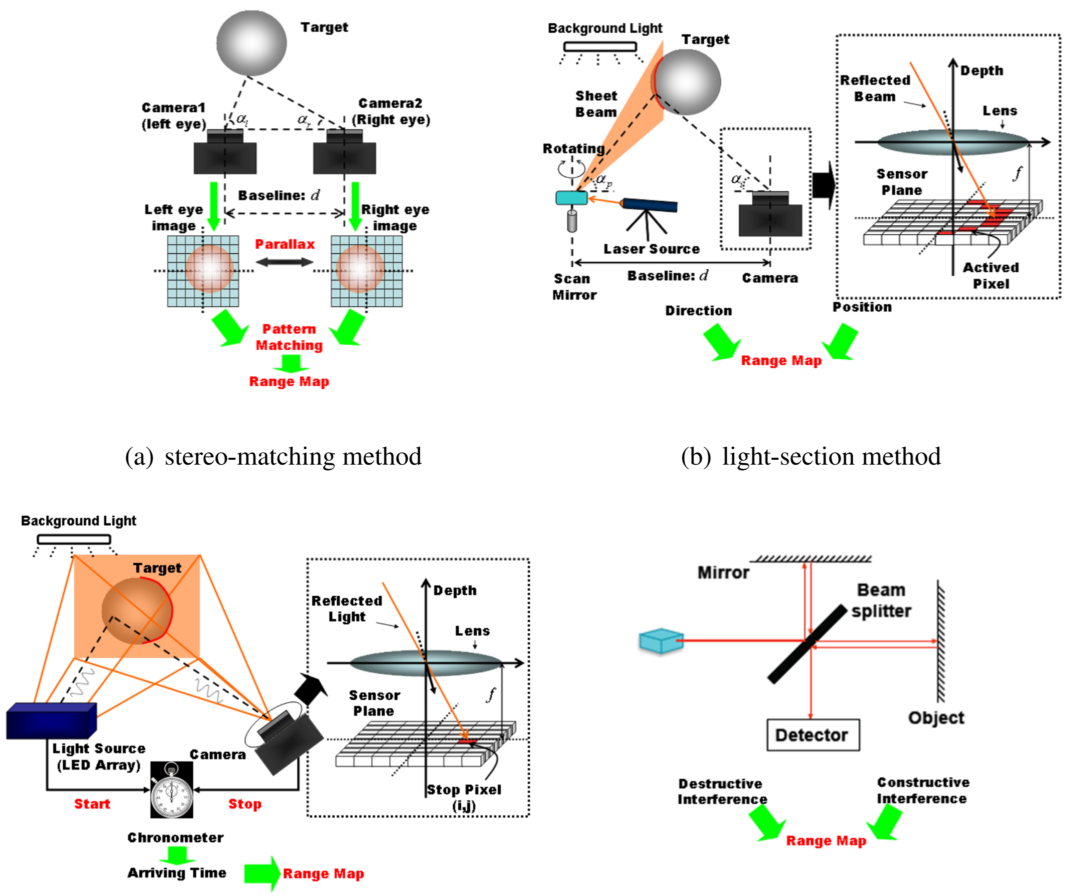

(a) stereo-matching method

(b) light-section method

(c) time-of-flight method

(d) interferometry method

Figure 1.2 Typical 3-D measurement methods:(a)stereo-matching method, (b)light-section method,(c)time-of-flight method,(d)interferometry method

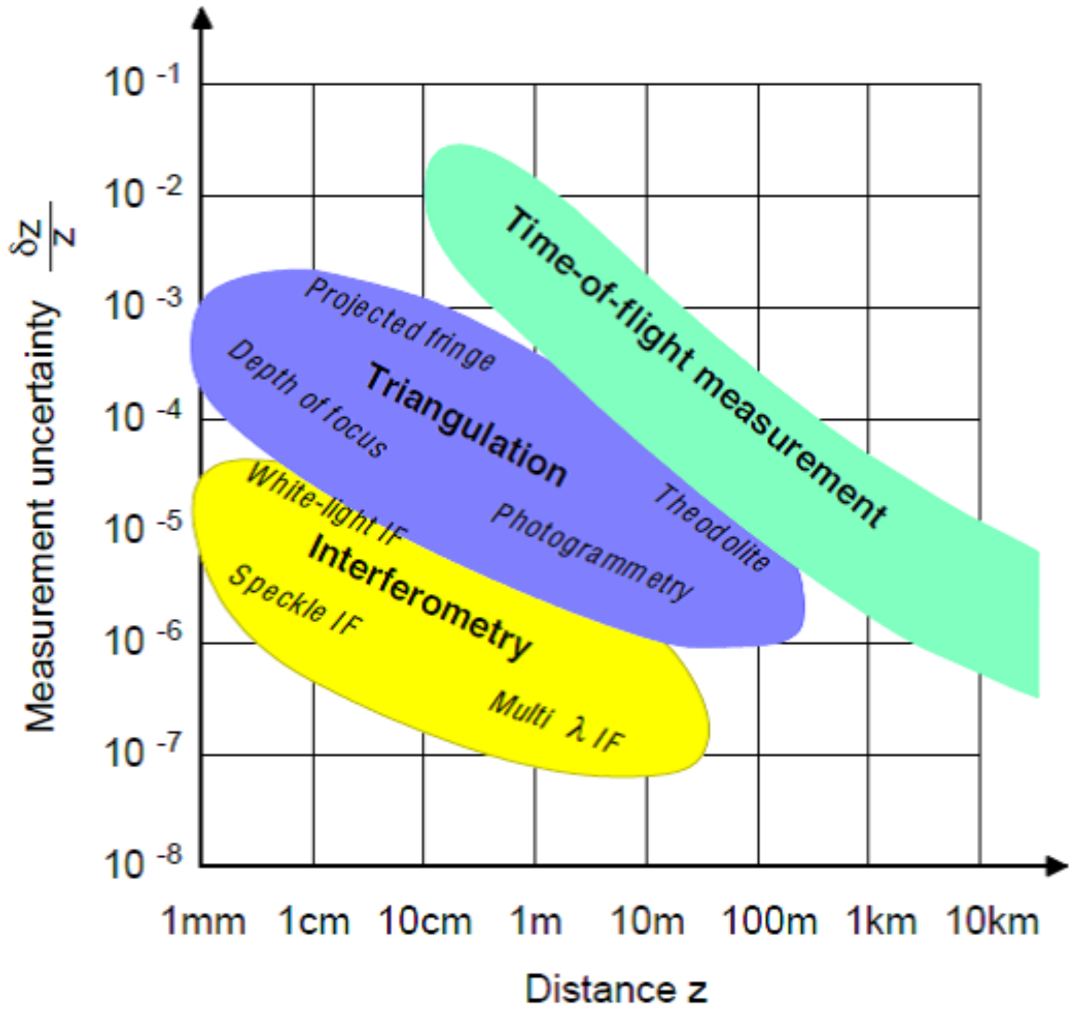

Figure 1.3 Performance map of conventional 3-D Measurement systems[22]

tions. And also, in the implementation level there are still so many issues we have to face. Among these issues the solution for background light is commonly a big challenge for many systems, especially for those systems using light-section and time-of-flight methods. The effects of suppression of background level will extremely influence the performance of the system such as sensitivity and range accuracy. So the evaluation of background light suppression characteristics of the systems is needed and important. Range accuracy which stands for the range finding capability of the system is also need to be evaluated. Never the less, there have been so many evaluation methods which could evaluate these two items existed in the earth. Actually they have so many problems. For example, ones only evaluate the range

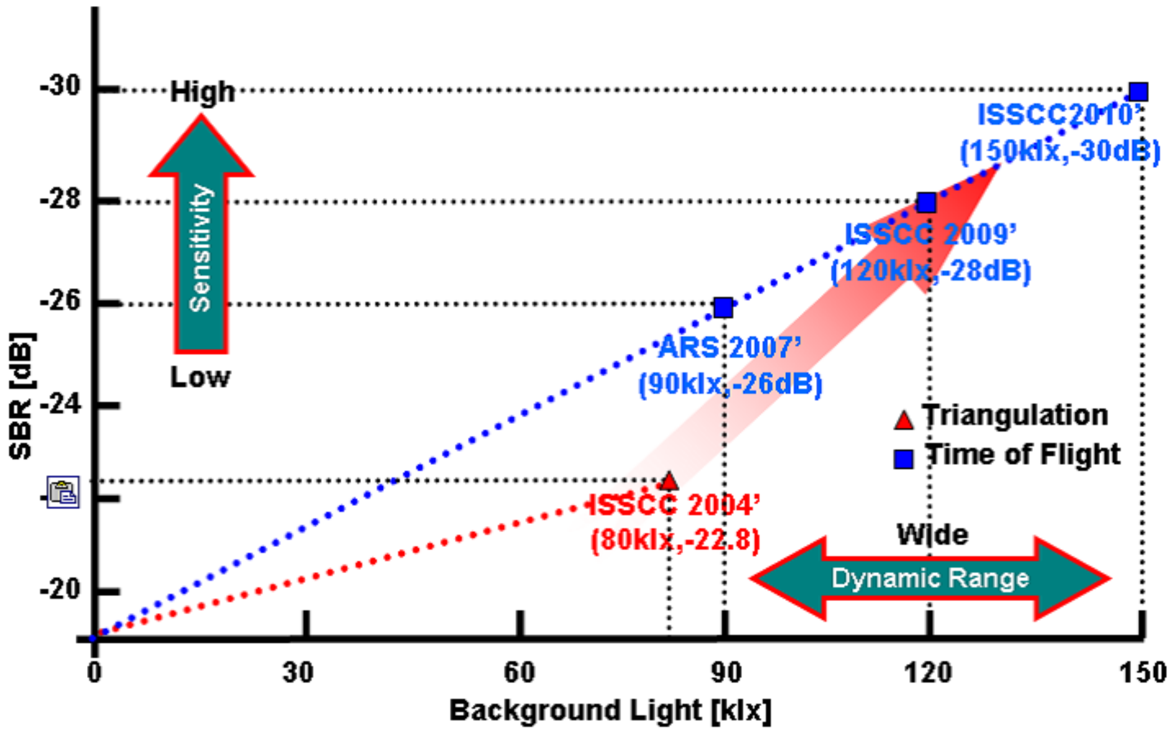

Figure 1.4 Performance map of 3-D Measurement systems with Smart image sensors in Background light

accuracy of the range finding systems in a fixed background light level. another ones only evaluate the range accuracy when the intensity of the signal light is fixed. Further more, ones only evaluate the Signal-to-background Ratio(SBR) which stands for the sensitivity of light detection of the range finding systems in a fixed background light level. another ones only evaluate the SBR when the intensity of the signal light is fixed. Although the results of these evaluation methods shows some level of the performance of the range finding systems, they are still not comprehensively enough to show the performance of the range finding systems because all of these system work in a variable background light level environment, and have to conquer different signal light intensities. Fig. 1.4 shows a comparison in terms of the level of background light and Signal-to-Background Ratio which stands for the sensitivity of light detection for some works in recent year. Thus, comprehensively evaluation methods for background light suppression characteristics and range accuracy are necessary and important.

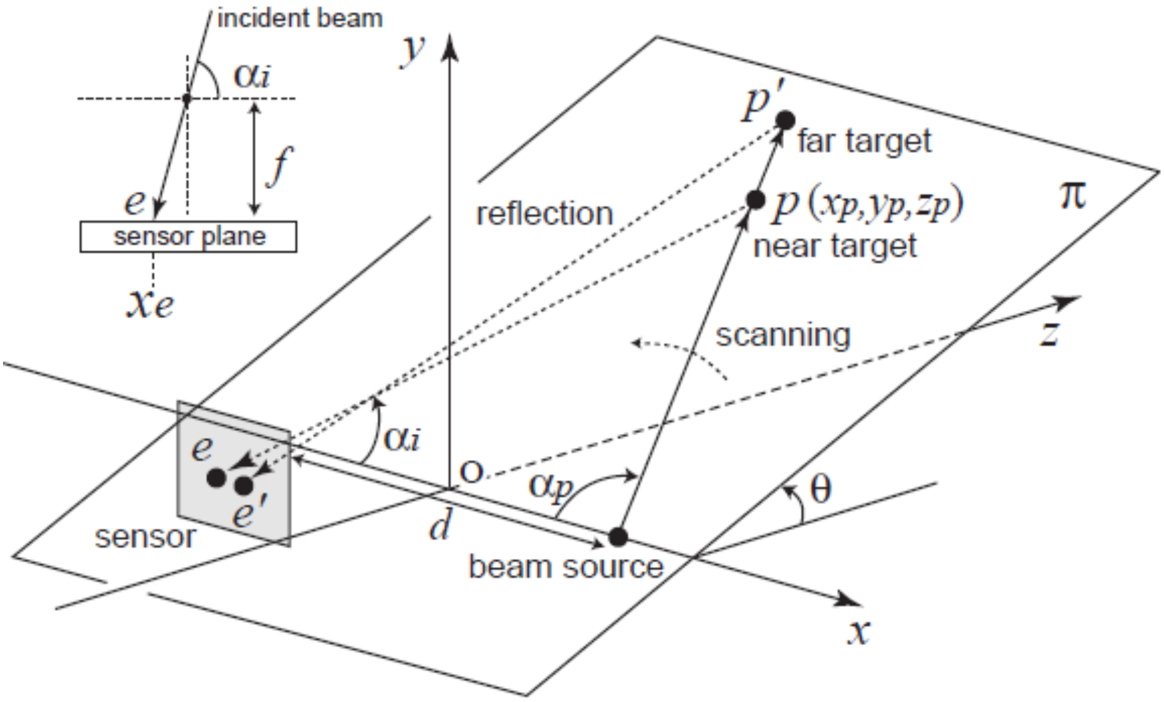

Figure 1.5 Principle of triangulation-based range calculation[58]

1.2 Main Range Finding Methods

As we have mentioned in background of this research, the triangulation method has a capability of high range accuracy in the middle-range target scene, and Time-of-Flight is efficient to capture in the wide-range target scene. In this section, we will explain the basic principle of light-section method and Time-of-Flight.

1.2.1 Light-Section Method

The light-section method can be categorized into triangulation method. For acquiring range map of the target scene, a laser light source modulated to sheet line is used and a image sensor detects the reflected laser light. Fig. 1.5(a)(b) shows the x-z plane and y-z plane respectively. Angles between sheet laser and x-axis, between reflected laserand x-z plane, and between reflected laser and y-z plane are a_p,a_p and θ respectively. Distances between the center of lens and target x address on the sensor plane, and the center of lens and target position on y-z plane are x and l respectively. Target position is (x_p, y_p,z_p), and baseline and focus of lens are d and f respectively. Then a_p and θ are given by

$$\tan a_i = \frac{f}{x_e} \tag{1.1}$$

$$\tan \theta = \frac{f}{y_e} \tag{1.2}$$

where *f* is a focal depth of a camera. a_i and a_p are also represented by

$$a_p = \frac{l}{d/2 - x_p} \tag{1.3}$$

$$a_i = \frac{l}{d/2 + x_p} \tag{1.4}$$

where *l* is a length of a perpendicular line from a target position, p, to x-axis. Therefore, x_p and *l* are given by

$$x_p = \frac{d(\tan a_p - \tan a_i)}{2(\tan a_p + \tan a_i)} \tag{1.5}$$

$$l = \frac{d \tan a_p \tan a_i}{2(\tan a_p + \tan a_i)} \tag{1.6}$$

Here, $y_p = lsin\theta$ and $z_p = lcos\theta$. Thus, y_p and z_p are also given by

$$y_p = \frac{d \tan a_p \tan a_i \sin\theta}{2(\tan a_p + \tan a_i)} \tag{1.7}$$

$$z_p = \frac{d \tan a_p \tan a_i \cos\theta}{2(\tan a_p + \tan a_i)} \tag{1.8}$$

1.2.2 Time-of-Flight(TOF) Method

Fig. 1.5 shows the simplest implementation of a time-of-flight range finding system using laser light source. The illumination is switched on for a very short time, the resulting light pulse illuminates the scene and is reflected by the objects. The lens of image sensor gathers the reflected light and images it onto the sensor plane. Depending on the distance, the incoming light experiences a delay. As light has a speed of *c* , this delay is t_d: an object distance,*d* , is given by:

$$d = \frac{c * t_d}{2} \tag{1.9}$$

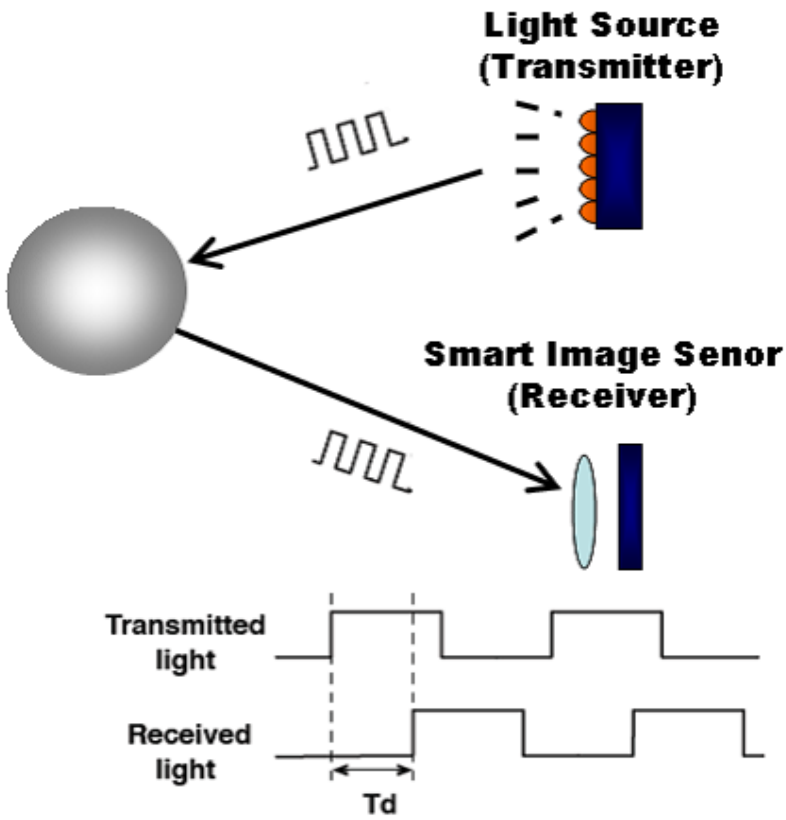

Figure 1.6 Principle of TOF-based range calculation

1.3 Smart Image Sensors

Image sensor is commonly a key component for 3-D measurement systems. As a maturated technology, Charge coupled device(CCD) was commonly used because of high sensitivity and strength to noise. However, CCD manufacturing process is complicated and hard to implement. Recent year with the rapid development of Complementary Metal Oxide Semiconductor(CMOS) technology which is similar to CCD. More and more image sensor for 3-D measurement using CMOS technology have been presented. Most remarkable point of CMOS image sensor is that CMOS image sensor transfer signal after amplifier, so that it is strong to circuit noises. Moreover, in CMOS image sensor, various circuit can be implemented with imaging device(photo-diode). In the conventional CMOS image sensor, a pixel array and signal processor are separated as shown in Fig. 1.7(a). However, there are many CMOS image sensor employing column-parallel signal processor and pixel-parallel signal

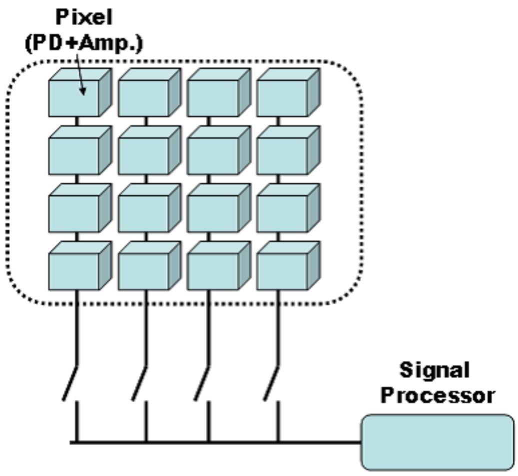

(a) a conventional signal processor

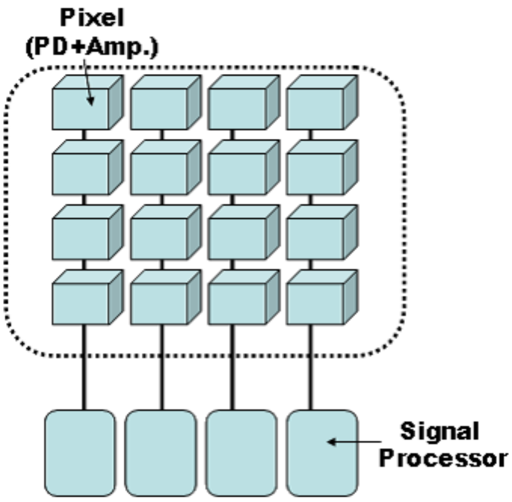

(b) a column-parallel signal processor

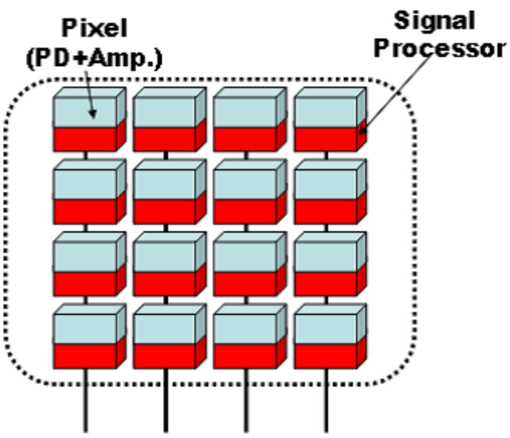

(c) a pixel-parallel signal processor

Figure 1.7 Imaging system configuration:(a)a conventional signal processor, (b)a column-parallel signal processor,(c)a pixel-parallel signal processor

processor as shown in Fig. 1.7(b)(c).

1.4 Thesis Organization

This work is subdivided into six chapters. **chapter 2** we describe four typical smart image sensors for 3-D Measurement base on different methods which we introduced in chapter1. The first one is a high speed and high accurate image sensors with light-section method. The basic idea and work principle is introduced in detail. The second one is a high dynamic range and high background Light suppression image sensors with light-section Method. The basic idea and work principle is also introduced in detail. The third one is a Time-of-Flight image sensor with lock-in pixel structure. The basic idea and work principle of it is introduced in detail. The last one is a Time-of-Flight image sensor with single-photon avalanche diodes. The basic idea and work principle is introduced in detail. In **chapter 3** ,base on the smart image sensors for 3-D Measurement we mentioned in chapter2, we discuss the problems of the existing evaluation method of the high speed and high accurate image sensors with light-section method and the high dynamic range and high background Light suppression image sensors with light-section Method which were mentioned in chapter2, and gives the evaluation method of background light suppression characteristics and range accuracy of both of the two images sensors. The evaluation results are summarized at the last of the chapter. In **chapter 4**, the problems of the existing evaluation method of the Time-of-Flight image sensor with lock-in pixel structure and the Time-of-Flight image sensor with single-photon avalanche diodes which were mentioned in chapter2 are discussed, and gives the evaluation method of background light suppression characteristics and range accuracy of both of the two images sensors. The evaluation results are summarized at the last of the chapter. **chapter 5** gives conclusion of this thesis.

Chapter 2

Smart Image Sensors for 3-D Measurement

In this chapter for finding out the comprehensive evaluation methods for background light suppression characteristics and range accuracy. We take four types of smart image sensors for 3-D measurement as our base. The first one is a high speed and high accurate image sensors with light-section method[31] which using multi-sampling principle to acquire the high accuracy. The second one is a high dynamic range and high background Light suppression image sensors with light-section Method[27] which using low-pass-filter to suppress background light and using demodulate principle to acquire high dynamic range. The third one is a Time-of-Flight image sensor with lock-in pixel structure[12] which using demodulate principle to detect the signal light. The last one is a Time-of-Flight image sensor with single-photon avalanche diodes [11] which also having a typical structure to acquire the flighting time of the signal light. In this chapter, we introduce the concepts and work principles of them.

2.1 High Speed and High Accurate Image Sensors with Light-Section Method

In this section, we will analysis a typical and conventional image sensor with light-section method. This image sensor totally and purely used the light-section method with a typical pixel circuit. The sensor acquired high speed and high accurate by using the special activated pixel scan technology and multi-sampling technology. For a purely light-section method, Fig. 2.1 shows the relation between background light and signal light for a conventional light-

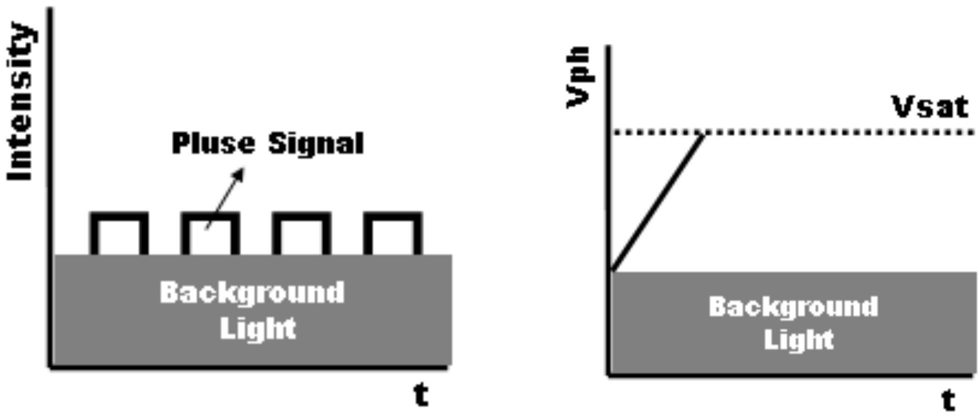

(a) (b)

Figure 2.1 Background Light with Signal Light for a conventional light-section method used smart image sensor(a)Detectable Signal Light in Background Light, (b)Voltage Level corresponding to Background Light and Signal Light

section method used smart image sensor. As shown in Fig. 2.1(a), the conventional smart image sensors using light-section method can only detect the signal light which intensity is stronger than the background light intensity. If the intensity of the signal light is not strong enough, no signal will be detect. In the case the signal light intensity is stronger than background light intensity, at the pixel level, the voltage correspond to the signal light intensity V_{ph} correspond to the incident signal light intensity is almost linear before the pixel saturate with the voltage V_{sat} as shown in Fig. 2.1(b).

Fig. 2.2 shows the pixel scheme of this image sensor. As shown in Fig. 2.2, the pixel is composed of a photodiode, a source follower, a transistor works as a reset switch, and well capacity C_{pd} and an AD converter. The output of photodiode V_{out} can be calculated by using photon-current I_{pd}, the integration time of the pixel t and the well capacity of the pixel C_{pd}, the photon-current includes two components I_{sig} caused by the signal light and I_{bg} caused by the background light. The output V_{pd} is given by

$$V_{pd} = \frac{I_{pd} * t}{C_{pd}} = \frac{(I_{sig} + I_{bg}) * t}{C_{pd}} \tag{2.1}$$

Here, the output voltage can be divided into V_{sig}, V_{bg} and V_{noise} corresponding to the signal

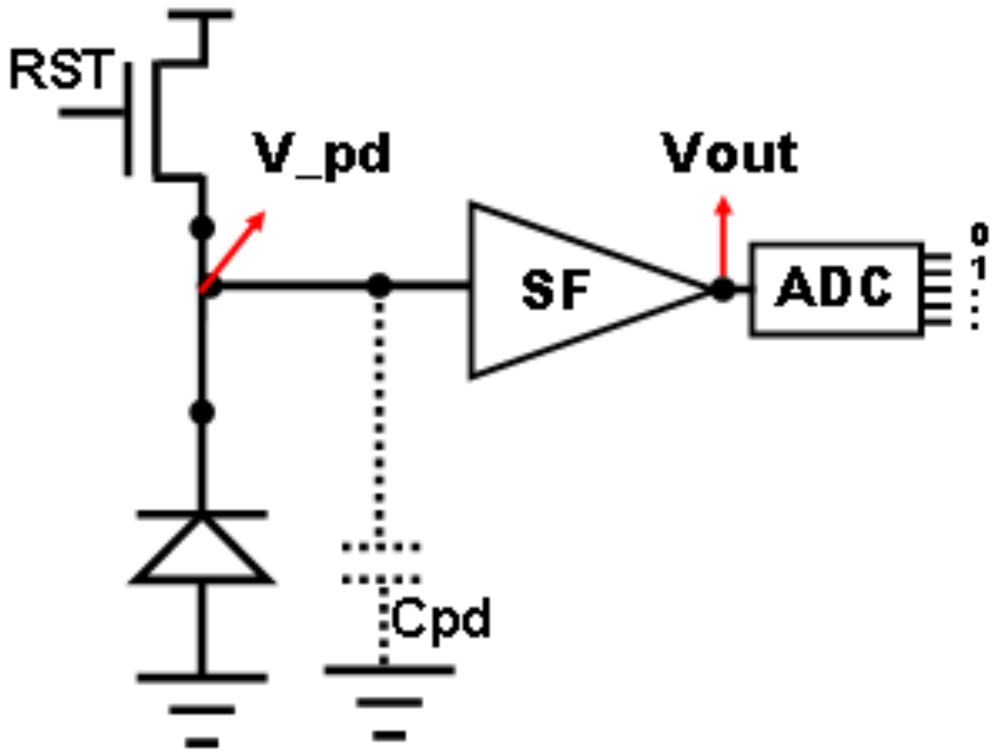

Figure 2.2 Pixel Scheme

light, background light and another noises respectively.

$$V_{pd} = V_{sig} + V_{bg} + V_{noise} \tag{2.2}$$

The signal intensity can be detected in the condition

$$V_{sig} + V_{bg} + V_{noise} \leq V_{sat} \tag{2.3}$$

And, take the gain of the source follower in consider, the output voltage V_{out} after amplified is given by

$$V_{out} = A_{sf} * (V_{sig} + V_{bg} + V_{noise}) \tag{2.4}$$

For finding the range data the sensor commonly composed of an array of pixels.The range data is calculated by the beam projection angle α_i and α_i the incident angle as shown in Fig.

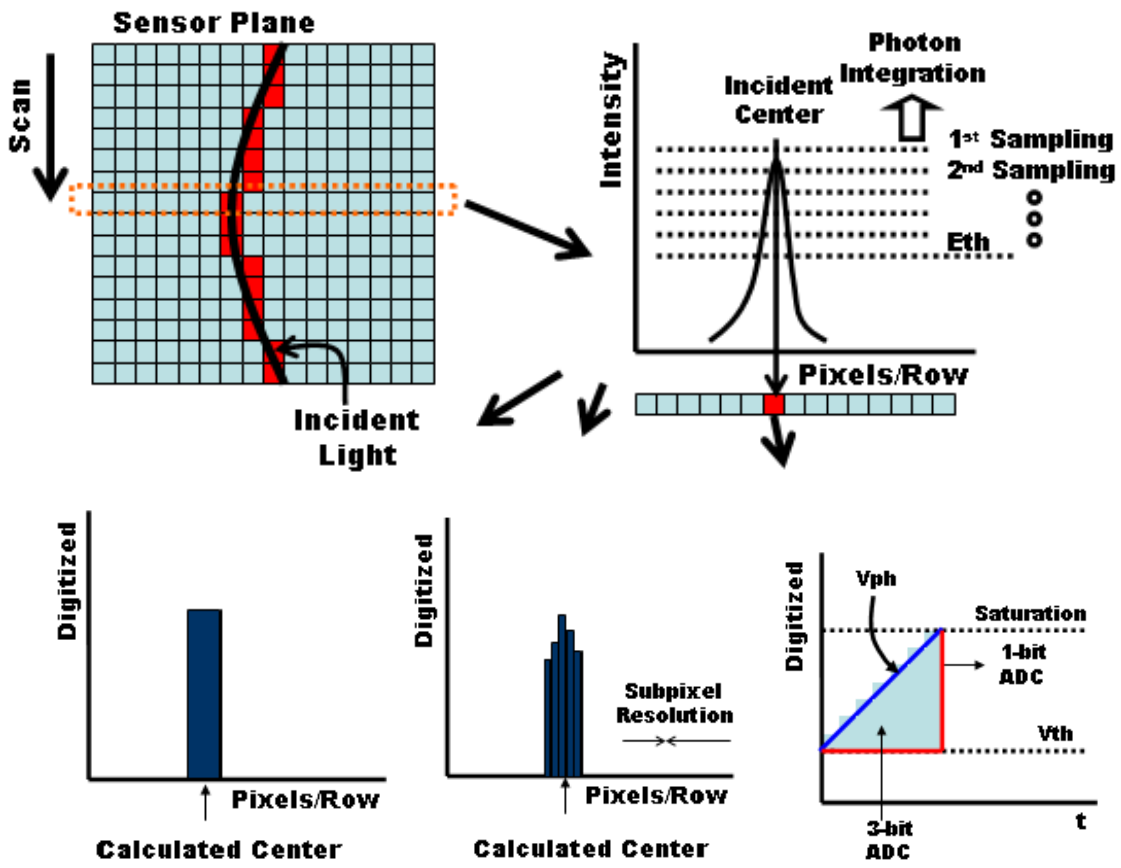

(a) Single-sampling method (b) Multi-sampling method (c) a pixel-parallel signal processor

Figure 2.3 Sub-pixel center position detection:(a)Single-sampling method, (b)Multi-sampling method,(c)using 1-bit and 3-bit ADC

1.2(b). The incident beam angle is provided from the incident beam position on the focal plane. Therefore, the range resolution and accuracy depend on the resolution of position detection on the sensor. In other words, the sub-pixel resolution efficiently improves the range accuracy. A multi-sampling technique is implemented to acquire the intensity profile of incident beam for a fine sub-pixel resolution. In a multi-sampling method, all the pixel values are updated repeatedly during the photo integration. Pixels with stronger incident intensity are activated faster and found many times in multiple samplings as shown in Fig. 2.3. In the conventional single sampling mode, the acquired data are binary, and so the sub-pixel resolution of calculated center position is 0.5 pixels as shown in Fig. 2.3(a). On the other hand, the number of samplings represents the scale of the intensity profile as shown in Fig. 2.3(b).The resolution of AD converter is quite a factor which will affect the range finding accuracy as shown in Fig. 2.3(c). If the AD converter has a higher resolution, the output of the pixel V_{out} can be expressed more precisely. So as a input to AD converter V_{out}, with the consideration of resolution of AD converter ΔV_{ADC}, the output of converter V_{pix} is given by

In this system, a laser pulse is used as a light source, so we can assume this optical pulse as a Gaussian shape. V_i is the voltage value at the location i, x_{real_peak} is the real peak location on the sensor plane and σ characterizes the pulse width.

$$V_i = V_{sig} * e^{\frac{-\left(x_i - x_{real\_peak}\right)^2}{2*\sigma^2}} \tag{2.5}$$

to determine the value of peak x_{cal_peak}, x_{cal_peak} may be estimated by using the centroid algorithm

$$x_{cal\_peak} = \frac{\sum_{i=1}^{N} V_{sig} * e^{\frac{-\left(x_i - x_{real\_peak}\right)^2}{2*\sigma^2}} * x_i}{\sum_{i=1}^{N} x_i} \tag{2.6}$$

Finally, to evaluate the accuracy of peak detection, we use the function give by

$$\Delta x_{peak} = |x_{cal\_peak} - x_{real\_peak}| \tag{2.7}$$

2.2 High Dynamic Range and High Background Light Suppression Image Sensors with Light-Section Method

As we discussed in section. 2.1, the conventional smart image sensors using light-section method can only detect the signal light which intensity is stronger than the background light intensity. That means even for a common background light environment such as in door at the day time. Extremely strong light source is needed. These types of laser light are commonly not safe to human eyes. As shown in Fig. 2.4, people want to find range finding systems can work in a strong background light level and also can work with a safe to human light source. To solve this problem, people have to suppress the background level with special ways such as

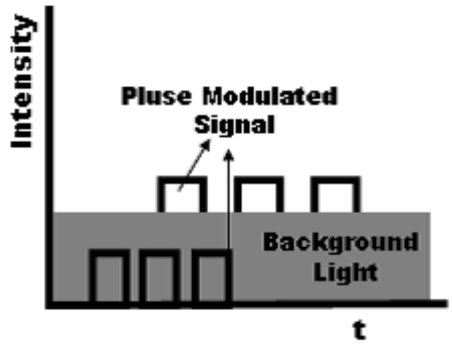

Figure 2.4 Background Light with Signal Light for a demodulation method smart image sensor by light-section method[31]

using a bandwidth filter or a electrical suppression method. Also, demodulation method can be used combine with the light-section method and using a modulated light source to detect the signal light to acquire a high selectivity for the range finding system. Fig. 2.5 illustrates a sensing scheme for high-sensitivity and wide-dynamic-range photo detection. In the light-section range finding system, a laser beam modulated by a pulse generator is projected on a target object. The photo detector receives a reflection of the projected laser beam and the background illumination together. A photo current generated by the incident light is fed into a low-pass filter. An output current of the low-pass filter is subtracted from the original photo current. The subtraction is realized using a current mode circuit instead of a voltage mode circuit in [85] to avoid saturation. The output current is alternating when the incident light includes a modulated light. A circuit limits the amplitude of current swing to avoid a saturation problem of a correlation circuit after the constant current suppression. The limited current swing is divided into two integrators by an external correlation signal. A marked difference voltage between the outputs of each integrator is acquired only when the incident light has the correlation frequency. The low-pass filter and the current-mode subtraction circuit realize the adaptive suppression of constant illumination. The logarithmic-response circuit and the correlation circuit are dedicated to wide-dynamic-range and high-sensitivity photo detection.

Fig. 2.6 shows a pixel circuit implementation of the present demodulation sensing. The

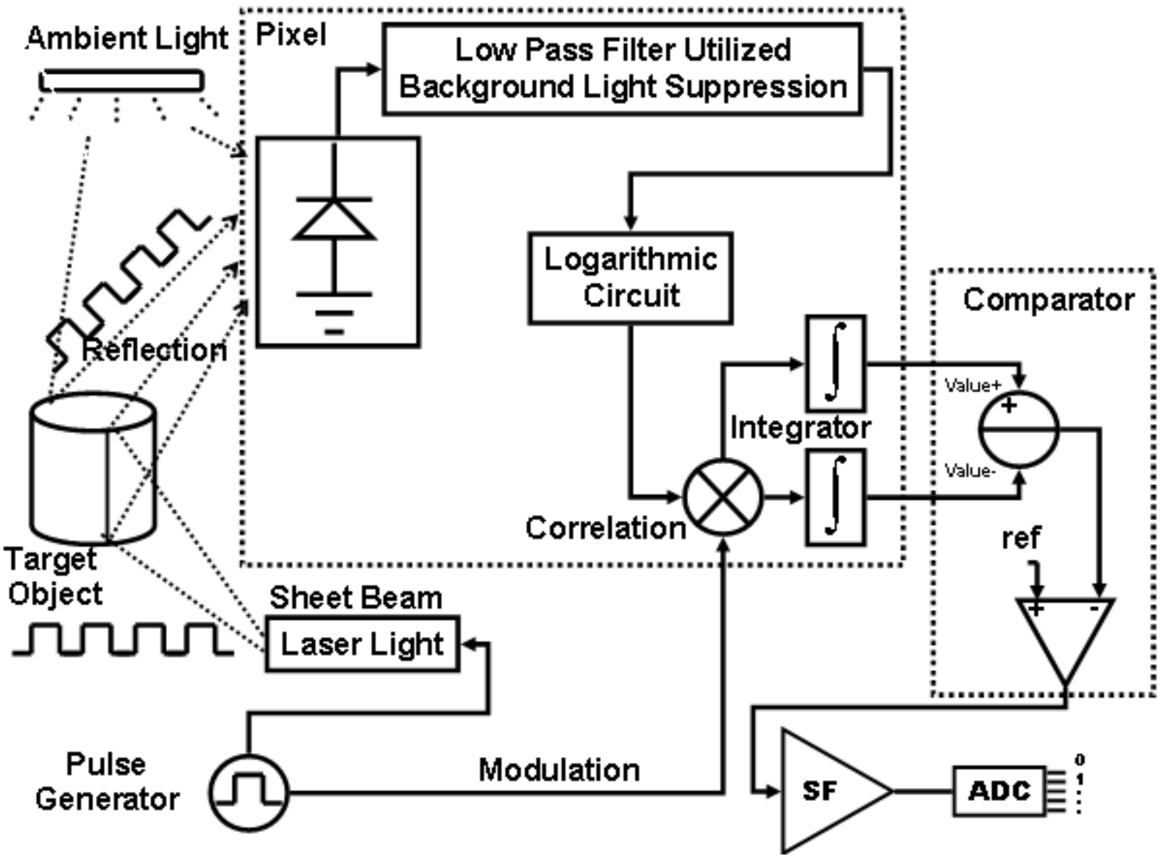

Figure 2.5 Basic idea of the demodulation sensing

pixel consists of a photo diode, a current-mode suppression circuit with low-pass filters, a bias circuit for the low-pass filters, a logarithmic I-V converter, two integrators for correlation, and two source follower circuits for readout. The transistor size (W/L) is also shown by micrometers (μm) in Fig. 2.6. The size of coupled or cascaded transistors is omitted in Fig. 2.6 since they are the same size. A photo current of I_{pd} is generated in proportion to the incident light intensity. The photo current is copied as a current of αI_{PD}, where α is a gain of the current copier circuit. Its average current, αI_{avg}, is generated by a low-pass filter and it is subtracted from αI_{PD}. The low-pass filter consists of two biased transistors (M_0 and M_1) and two capacitors (C_0 and C_1). The biased transistors are used for a resistor of the low-pass filter, which are based on HRES (Horizontal RESistor) presented in [86]. A drain-source current, I_{M0}, of the transistor, M_0, is controlled by the gate voltage of V_{g0}. The bias circuit makes the gate-source voltage of V_q constant in each pixel for constant resistance. The

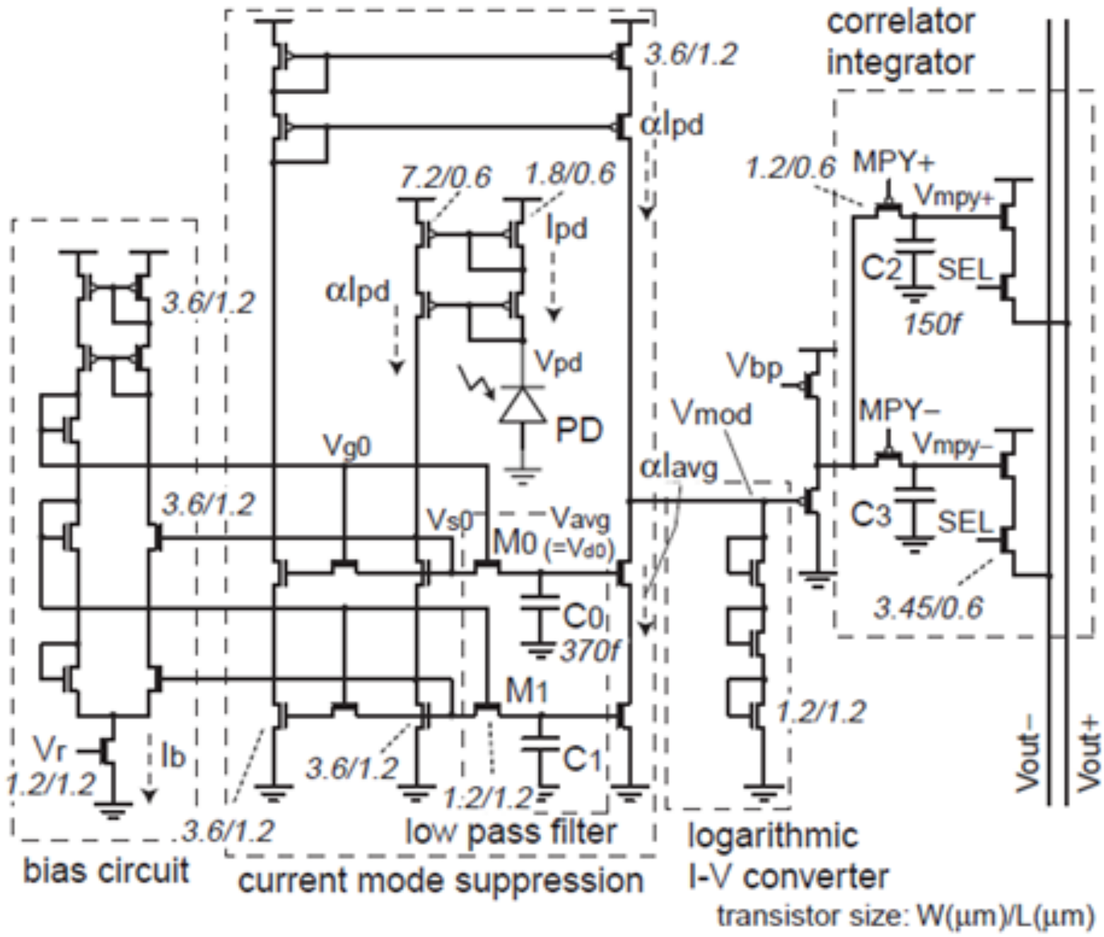

Figure 2.6 Pixel circuit implementation of the demodulation sensing[31].

saturation current of the biased transistor, M_0, is half of the bias current of I_b controlled by V_r.

Fig. 2.7 shows a timing diagram of the pixel circuit operation. Here, f_0 is a correlation frequency. When the incident light includes a modulated light, the photo current, I_{PD}, has two components of a constant current of I_{dc} by an Background light and an alternating current of I_{ac} by a modulated light.

$$I_{pd} = I_{dc} + I_{ac} \tag{2.8}$$

The low-pass filter generates the average current, αI_{avg}, as follows.αI_{avg}

$$\alpha I_{avg} = \alpha \overline{I_{pd}} = \alpha \left(I_{dc} + \overline{I_{ac}} \right) \tag{2.9}$$

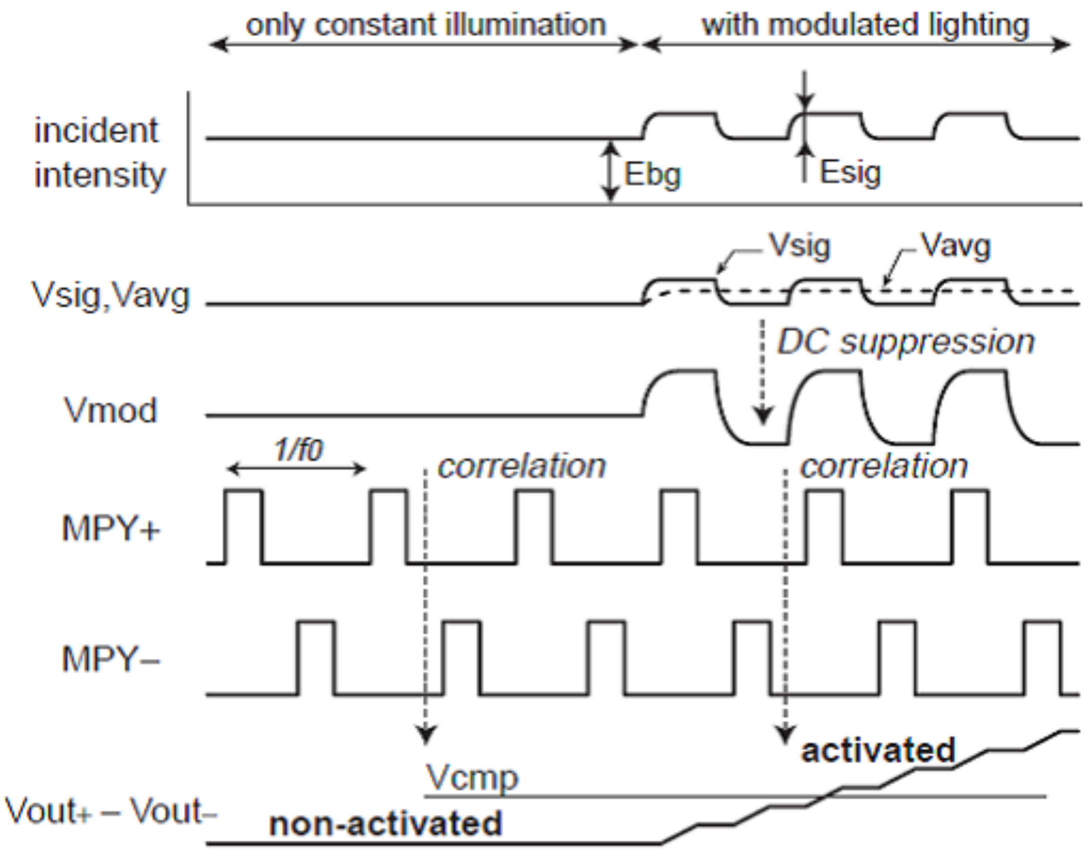

Figure 2.7 Timing diagram of the pixel circuit operation[31].

The constant current, I_{dc}, is adaptively suppressed by the current-mode suppression circuit. Here, a time constant of the low-pass filter is designed at 1.2 ms in a typical situation. It can be adjusted by the external bias voltage, V_r. The output current, I_{mod}, of the suppression circuit is given by

$$I_{mod} = \alpha' I_{dc} - \alpha I_{avg} \approx \alpha \left(I_{ac} - \overline{I_{ac}} \right) \tag{2.10}$$

The output current, I_{mod}, is converted to a voltage level of V_{mod} by a logarithmic-response circuit.

$$V_{mod} = \beta \log \left(I_{offset} + I_{mod} \right) \tag{2.11}$$

where β is a gain factor of the logarithmic-response circuit and I_0 is an offset current. The output is divided into two capacitors, C_2 and C_2, by the external signals, MPY+ and MPY-, synchronized with the correlation frequency. The voltages, V_{mpy+} and V_{mpy-}, at C_2 and C_2 are read out as V_{out+} and V_{out-} by source follower circuits, respectively. When the incident light contains only the background illumination, the photo current is constant and I_{mod} is zero. In this case, the difference voltage between V_{out+} and V_{out-} is zero, and the pixel is recognized as an inactive pixel. On the other hand, the marked difference between V_{out+} and V_{out-} is acquired only when the incident light has the frequency synchronized with the correlation signal. The pixel is recognized as an active pixel when the difference voltage exceeds the reference voltage, V_{cmp}, as follows.

$$V_{out+} - V_{out-} \geq V_{cmp} \tag{2.12}$$

By combing all the process we discussed before, the final output of the pixel can be given by

$$V_{out} = \sum_{i=1}^{N} \left(V_{out+} - V_{out-}\right) = \sum_{i=1}^{N} \beta \int_{t-T}^{t} \log I_{PD}\left(\tau\right) \Delta V_{MPY}\left(\tau\right) d\tau \tag{2.13}$$

As we discussed in section. 2.1, the resolution of AD converter is quite a factor which will affect the range finding accuracy. So as a input to AD converter V_{out}, with the consideration of resolution of AD converter ΔV_{ADC}, the output of converter V_{pix} is given by

In this system, a laser pulse is used as a light source, so we can assume this optical pulse as a Gaussian shape. V_i is the voltage value at the location i, x_{real_peak} is the real peak location on the sensor plane and σ characterizes the pulse width.

$$V_i = V_{sig} * e^{\frac{-\left(x_i - x_{real\_peak}\right)^2}{2*\sigma^2}} \tag{2.14}$$

to determine the value of peak x_{cal_peak}, x_{cal_peak} may be estimated by using the centroid algorithm

$$x_{cal\_peak} = \frac{\sum_{i=1}^{N} V_{sig} * e^{\frac{-\left(x_i - x_{real\_peak}\right)^2}{2*\sigma^2}} * x_i}{\sum_{i=1}^{N} x_i} \tag{2.15}$$

Finally, to evaluate the accuracy of peak detection, we use the function give by

$$\Delta x_{peak} = \left|x_{cal\_peak} - x_{real\_peak}\right| \tag{2.16}$$

2.3 Time-of-Flight Image Sensor with Lock-in Pixel Structure

In this section we will analysis a time-of-flight image sensor with a lock-in structure. A lock-in structure is a type of amplifier that can extract a signal with a known carrier wave from an extremely noisy environment (the signal-to-noise ratio can be -60 dB or even less. It is essentially a homodyne with an extremely low pass filter (making it very narrow band). Lock-in amplifiers use mixing, through a frequency mixer, to convert the signal's phase and amplitude to a DC-actually a time-varying low-frequency-voltage signal. The device is often used to measure phase shift, even when the signals are large and of high signal-to-noise ratio, and do not need further improvement. Recovering signals at low signal-to-noise ratios requires a strong, clean reference signal the same frequency as the received signal. This is not the case in many experiments, so the instrument can recover signals buried in the noise only in a limited set of circumstances. The lock-in amplifier was invented by Princeton University physicist Robert H. Dicke who founded the company Princeton Applied Research (PAR) to market the product. So one can use this structure as to detect the signal wave in complicate background condition. This work just benefit form this structure as a base of a demodulator. A special pixel structure was made to get this principle realized. Fig. 2.8 is the simplified layout of the pixel. TX1, TX2, TXD, and PG are polysilicon gates placed on field oxide. The photogate, PG is the photosensitive region of the pixel. Aside from PG, the other gates are used to control the direction of photoelectron flow according to their TOF. FD_1 and FD_2 are floating diffusions used to collect signal charges from PG through transfer gates TX1 and TX2, respectively. Unwanted background light induced photoelectrons are transferred to the two charge drains through the charge draining gates TXD.

Fig. 2.9(a) is the cross section of the pixel at line xx'. Here, it is shown howa source follower and a reset transistor are connected to each floating diffusion output node in order to systematically reset and read out the signal levels. The n-buried layer prevents photoelectrons to be captured by interface traps by creating a potential maximum in the bulk. The active illumination used is an array of infrared LEDs having a wavelength of 870 nm. At this wavelength, the penetration depth of photons is approximately 22 μm beneath the pixel 's surface [7]. To

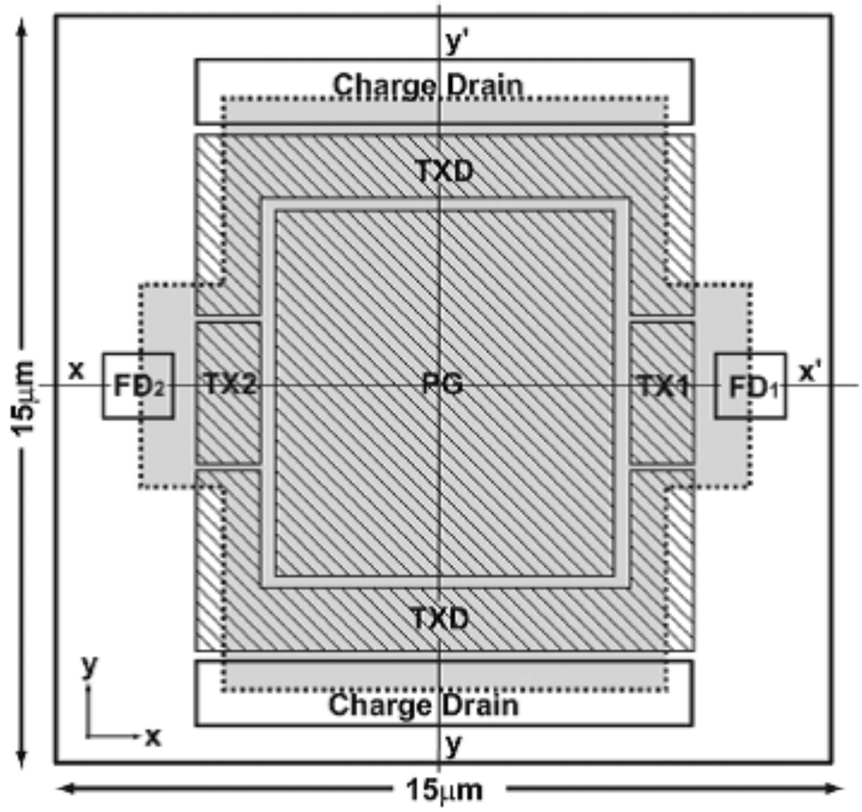

Figure 2.8 TOF pixel layout[12]

maximize the capture of moderately deep generated photoelectrons, a lightly doped p-type epitaxial layer is formed beneath the n-buried layer. This layer creates a vertical potential profile within the pixel. The resulting electric field from this potential gradient accelerates moderately deep generated photoelectrons to the surface at where it could be transferred to the output nodes. On the other hand, deep generated photoelectrons will migrate to the surface through thermal diffusion. Their arrival time from the deep regions of the pixel to the surface does not coincide with the TOF of the system thus contaminating the signal charge. To reduce their numbers, a highly doped p-type bulk material is used to increase the recombination rate of electrons.

Fig. 2.9(b) is the cross section of the layout at line yy'. Here, the charge draining structures are stressed. Background induced photoelectrons are transferred to the charge drains via gates TXD. The drains are connected to the supply rails which enable these photoelectrons to be drained safely out of the pixel.

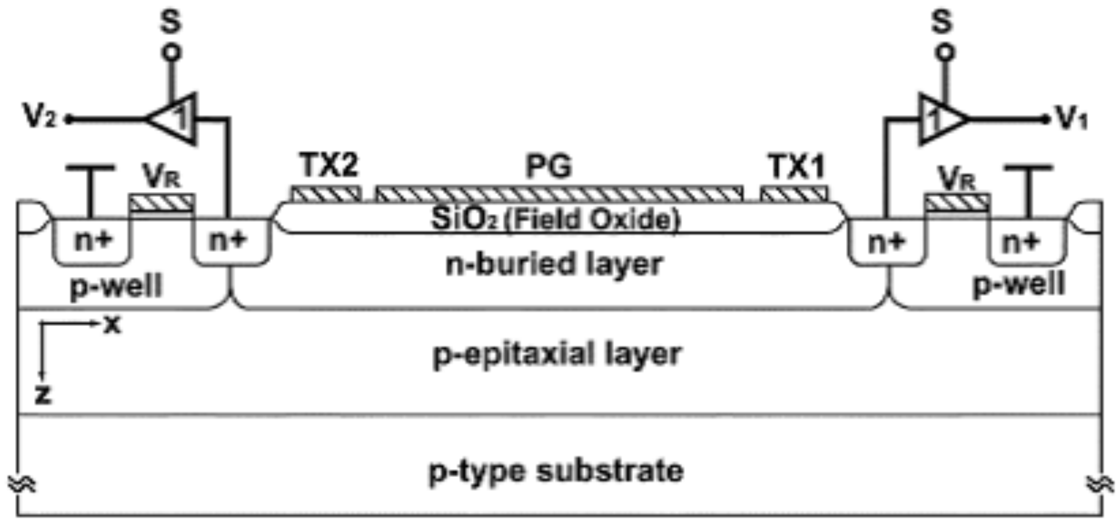

(a)

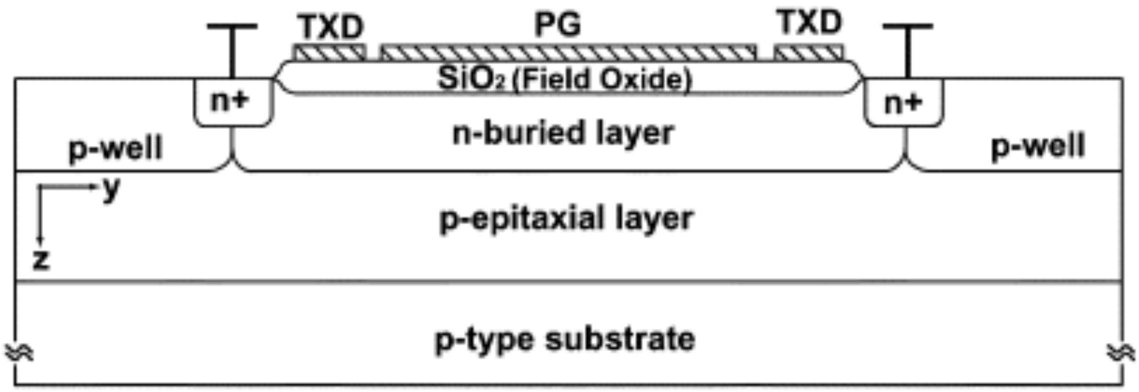

(b)

Figure 2.9 Pixel cross section:(a)X-plane, (b)Y-plane[12]

Fig. 2.10 shows the control pulses associated during TOF integration. Pulses ϕ_{TX1} and ϕ_{TX1} are used to transfer generated electrons to node FD_1 and FD_2, while is ϕ_{TXD} used to drain background light generated charge to the charge drains. The hatched boxes are used to show the amount of charge transferred to each floating diffusion node according to T_D. Each box corresponds to the overlapping region of the received light pulse with the pulse in PHASE1 and PHASE2. The TOF accumulation cycle is separated into three phases, namely, PHASE1, PHASE2, and PHASE3. These pulses are applied to the gates of the pixel. PG is held constantly at ground voltage both during accumulation and readout. The active illumination light

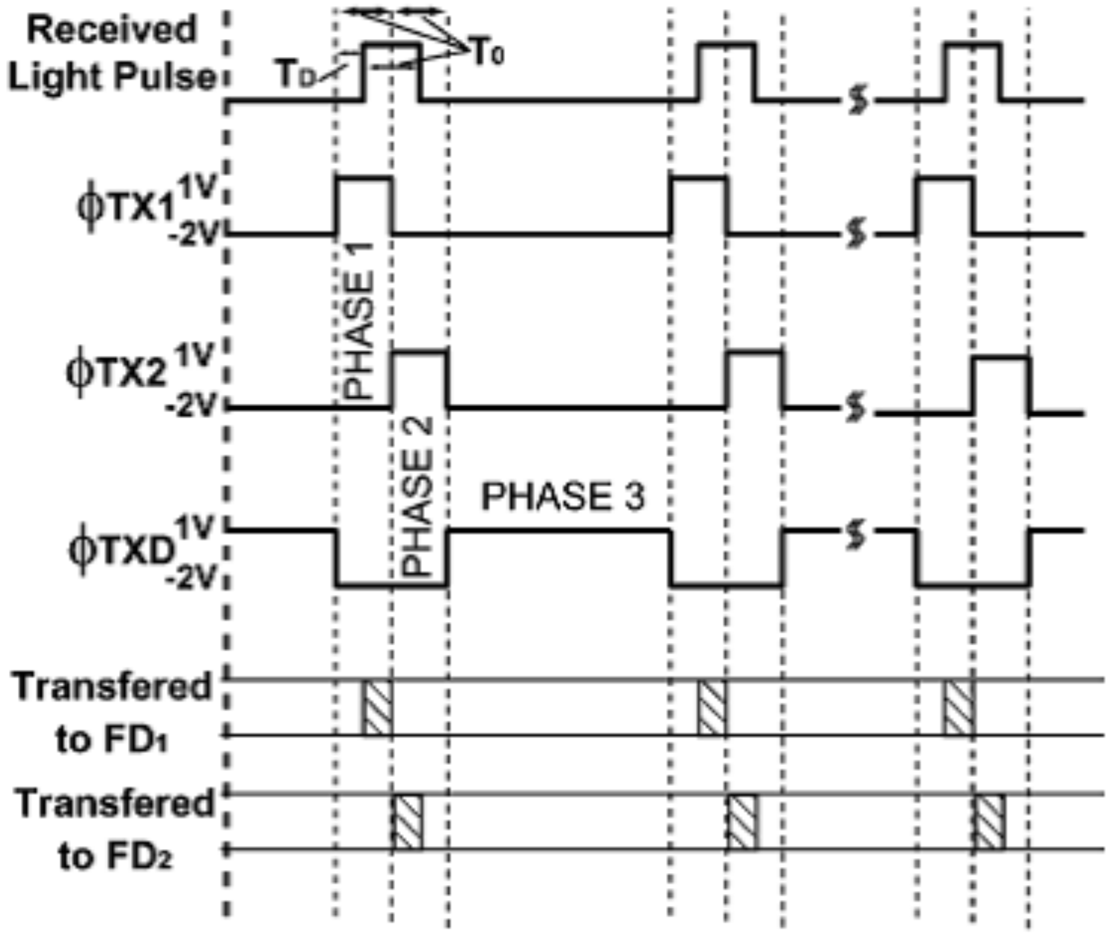

Figure 2.10 Pixel control pulses[12]

sources are pulsed with the same pattern ϕ_{TX1} as with a pulsewidth of T_0. A 10% duty cycle is used for the active illumination light source to ensure a high instantaneous emitted power and at the same time to increase the unwanted charge draining time. The received light pulses shown are delayed by its TOF of T_D causing delay dependent amounts of induced photoelectrons to be transferred to the output nodes V_1 and V_2.Charges are transferred for multiple times in order to obtain an adequate amount of signal charge.

Fig. 2.11 depicts how the pixel 's lateral surface potential is used to perform charge transfer and separation of the generated photoelectrons according to T_D. In Fig. 2.11(a), the resulting potential profile during PHASE1 and PHASE2 are shown using solid lines and dashed lines, respectively. In PHASE1, the potential profile sloping down towards V_1 results in an electric

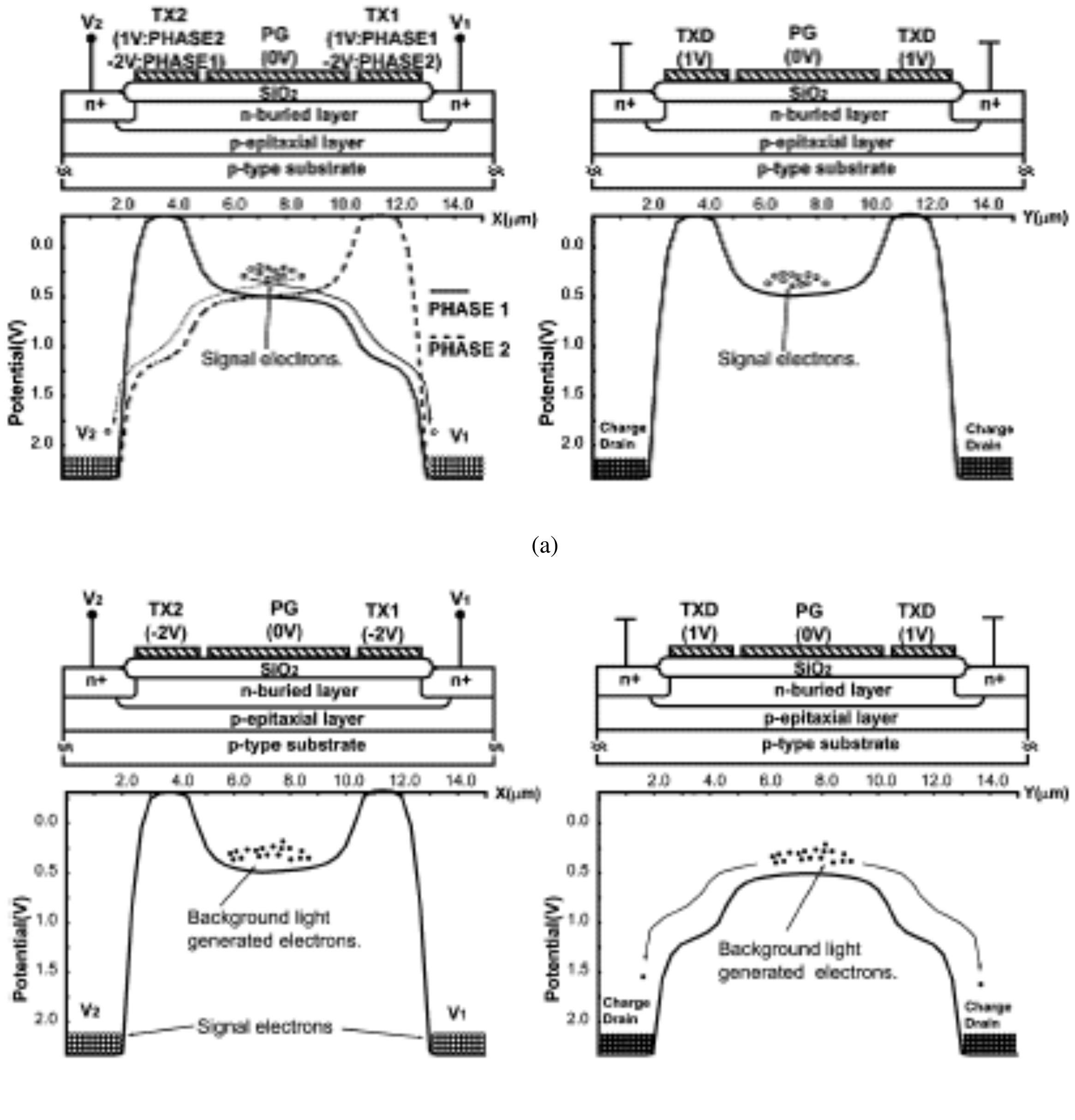

Figure 2.11 Charge separation during (a) PHASE1 and PHASE2. (b) PHASE3[12]

fields that quickly transfer the generated photoelectrons during this phase from their generation site under PG to V_1 through gate TX1. The same mechanism transfers photoelectrons to node V_2 in PHASE2. During these two phases, -2V is applied to TXD causing a potential barrier between PG and the charge drains. Fig. 2.117(b) shows the lateral potential profile in both the X and Y directions of the pixel during PHASE3. The photoelectrons generated during this phase are caused by background illumination. By applying -2V to TX1 and TX2, a potential barrier is created and it effectively isolates nodes V_1 and V_2 from the photogate where background generated photoelectrons are being generated. On the other hand, 1V is applied to both the charge draining gates to connect the charge drains with the photogate. The electric field during this phase accelerates the background induced photoelectrons to the charge drains that are constantly being connected to the power supply rails. Upon arriving in the charge drains, the photoelectrons are diffused safely out of the pixel. The same potential profile as in PHASE3 is used during signal readout to ensure isolation of the readout signal from background light generated noise.During the transfer of signal electrons in PHASE1 and PHASE2 to its respective output nodes, a photocurrent I_{ph} is induced. the amount of electrons transferred to node FD_1 and FD_2 is given by

$$N_1 = \frac{I_{PD}}{q}\left(T_0 - T_D\right) \tag{2.17}$$

and

$$N_2 = \frac{I_{PD}}{q}T_D \tag{2.18}$$

the photo current, I_{PD}, has two components of a constant current of I_{dc} by an Background light and an alternating current of I_{ac} by a modulated light.

$$I_{pd} = I_{dc} + I_{ac} \tag{2.19}$$

respectively. the TOF which directly corresponds to is written as

$$TOF = \frac{T_0 N_2}{N_1 + N_2} \tag{2.20}$$

and the measured range, L is given by

$$L = \frac{cT_0 N_2}{2\left(N_1 + N_2\right)} \tag{2.21}$$

where is c the speed of light. If the output node capacitances are equal, the number of electrons collected can be replaced by their corresponding voltage level and 2.3 can be rewritten as

$$L = \frac{cT_0 V_2}{2\left(V_1 + V_2\right)} \tag{2.22}$$

by the lock-in principle, V_1 is give by

$$V_1 = \frac{1}{N}\sum_{i=1}^{N}\left(\int_{t-T}^{t} I_{C1}(t)\,dt - \int_{t-T}^{t} I_{C2}(t)\,dt\right) = \frac{1}{N}\sum_{i=1}^{N}\rho\int_{t-T}^{t} I_{PD}(t)\,V(t)\,dt \quad (2.23)$$

also, V_2 is give by

$$V_2 = \frac{1}{N}\sum_{i=1}^{N}\left(\int_{t-T}^{t} I_{C1}(t)\,dt + \int_{t-T}^{t} I_{C2}(t)\,dt\right) = \frac{1}{N}\sum_{i=1}^{N}\int_{t-T}^{t} I_{PD}(t)\,dt \quad (2.24)$$

An offset voltage V_{offset}, caused by deep generated electrons diffusing to the surface and modifying the measured signal voltage, must be taken into consider while we are calculating the range L, so L is give by

$$L_{cal} = \frac{cT_0\left(V_2 - V_{offset}\right)}{2\left(V_1 + V_2 - 2V_{offset}\right)} \quad (2.25)$$

To evaluate the range finding accuracy, we use the function give by

$$\Delta L_{peak} = |L_{cal\_peak} - L_{real\_peak}) \quad (2.26)$$

2.4 Time-of-Flight Image Sensor with Single-Photon Avalanche Diodes

Another way to acquire the time-of-flight is to use Single-Photon Avalanche Diodes as photon detector. In this section we will introduce and analyzed this Time-of-Flight image sensor with Single-Photon Avalanche Diodes. Solid-state single-photon detectors have existed for decades and, while several flavors of solid-state detectors exist in various technologies and ranges of operation, from cryogenic to room temperature detectors, silicon avalanche photodiodes (APDs) have emerged as the most versatile and easy to use among them [52]. A class of APDs operating above breakdown, in so-called Geiger mode and known as single-photon avalanche diodes (SPADs), is of particular interest due to their amenability to integration in planar silicon processes in combination with conventional digital and analog circuitries. The first SPADs implemented in a planar technology have emerged relatively recently [53],[54]. But, while the physics of solid-state SPADs is well understood [55], it is only with the advent of devices integrated in conventional CMOS processes [56], that the evolution onto smaller

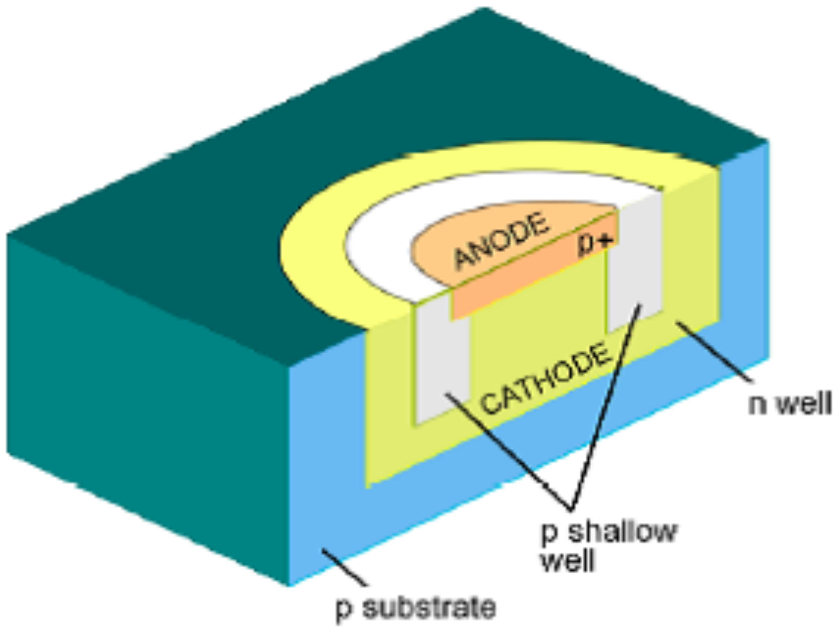

Figure 2.12 SPAD cross-section in a conventional CMOS process[57]

and smaller feature sizes has rapidly advanced to the point that it has now become possible to envision large imaging systems based on SPADs Fig. 2.12 shows the SPAD cross-section in a conventional CMOS process.

Fig. 2.13 shows the principle of a SPAD image sensor. When the light source project a signal light to the target object, a start signal will be sent to the Time-to-Digital Converter [39]-[51], then when the signal light reflected to the sensor plane, a SPAD will be triggered. The avalanche of SPAD will generate a pulse. As the stop signal this pulse will be sent to Time-to-Digital Converter as well. By using this two signal, the time-of-flight can be found out. Fig. 2.13 shows the the pixel scheme of a SPAD image sensor. As a key component, the resolution of time-to-digital converter determines the resolution of time-of-flight, and determines the range accuracy as well. The probability of false trigger caused by background light is given by

$$P_n(t;E) = exp(-t * \eta_0 * E) \tag{2.27}$$

E is the arriving rate of the photons caused by the background light. Thus, the density of

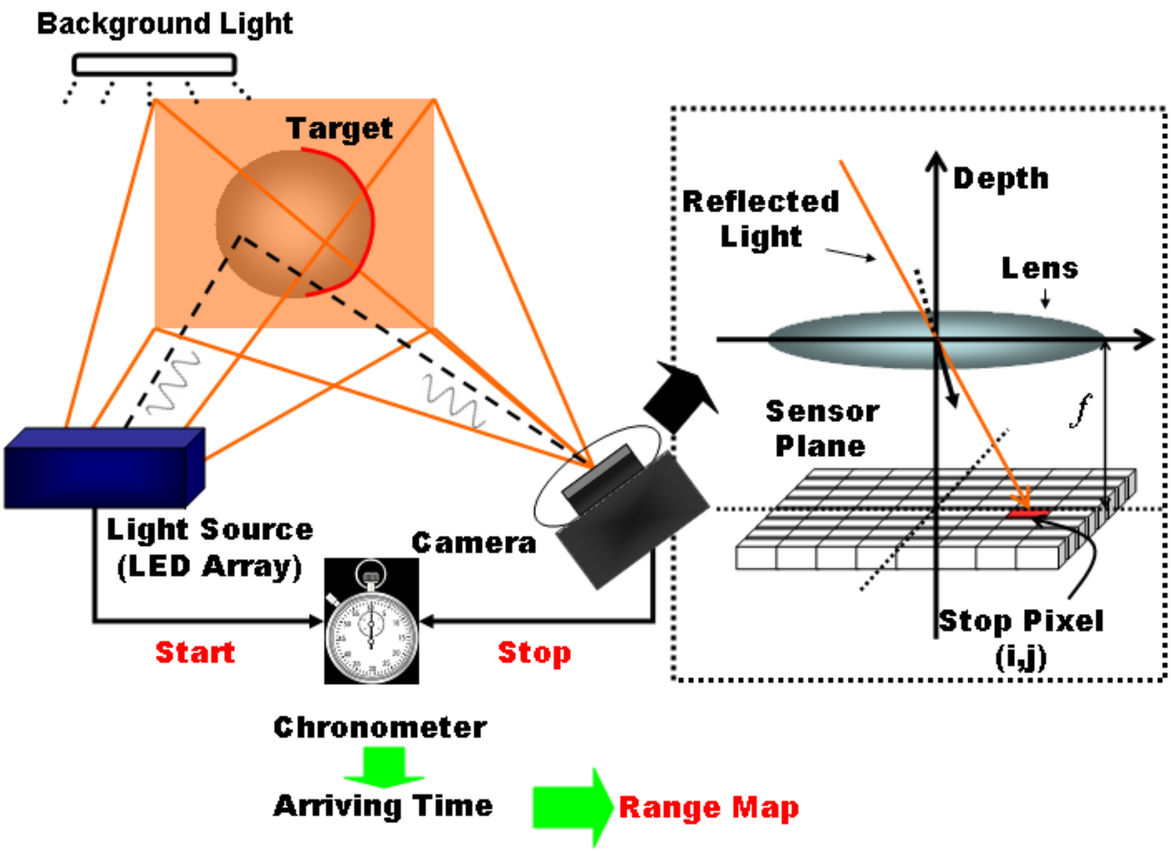

Figure 2.13 Principle of a SPAD image sensor

false trigger by background light is given by

$$\eta_0 * E \leq \tau^{-1} \tag{2.28}$$

Take the dead time t_{dead} of SPAD into consider. The probability of false trigger caused by background light is changed to

$$P_n(t; E) = exp(-min(t, t_{dead}) * \eta * E) \tag{2.29}$$

Also, the the density of false trigger by background light is changed into

$$\eta_0 * E \leq {t_{dead}}^{-1} \tag{2.30}$$

As a Gaussian shape signal, the signal return density can be give by,

$$r(t) = \frac{Q_r}{hv} * \frac{1}{\sqrt{2\pi} * \sigma} * exp(-t^2/2\sigma^2) \tag{2.31}$$

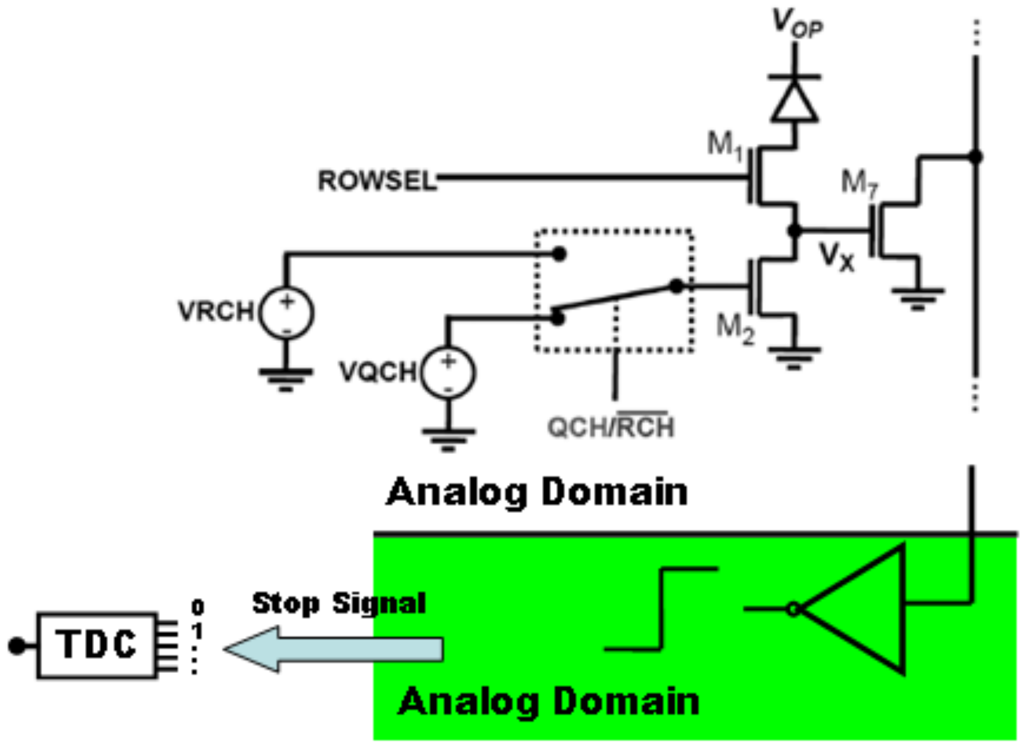

Figure 2.14 Pixel Scheme of a SPAD image sensor

where the Q_r is the power of the signal, and σ is the pulse width. h is the Plank's constant.

Thus the signal return probability can be given as

$$P_n(t; r(t)) = exp\left(\frac{-1}{2} * \frac{\eta_0 * Q_r}{hv}\left[erf\left(\frac{t}{\sqrt{2} * \sigma}\right) + 1\right]\right) \tag{2.32}$$

So the totally probability of background light and signal light is given by

$$h(t) = P_n(t; E) + P_n(t; r(t)) \tag{2.33}$$

Take the resolution of time-of-digital converter into consider. The time-of-flight is acquired by calculating the arriving time centroid of the light by

$$TOF = \frac{\sum_{i=TOF'-PW/2}^{TOF'+PW/2} h(t) * t}{\sum_{i=TOF'-PW/2}^{TOF'+PW/2} h(t)} \tag{2.34}$$

Chapter 3

Evaluation of Background Light Suppression Characteristic and Range Finding Accuracy for Light-Section Method

As we discussed and analyzed four typical types of image sensors: a high Speed and high accurate image sensors with light-section method, a high dynamic range and high background light suppression image sensors with light-section method, a Time-of-Flight image sensor with lock-in pixel structure and a Time-of-Flight image sensor with single-photon avalanche diodes in chapter 2. Actually all of this four image sensors have been evaluated in their works respectively, but for the evaluation of background light characteristics and range finding accuracy. The evaluations are not enough. From this chapter we will discuss the problems of the existing evaluation for them respectively, and towards the problems we will present our method to solve the existing problems and provide a new respect to evaluate the image sensors for 3-D measurement.

3.1 Evaluation of High Speed and High Accurate Image Sensors with Light-Section Method

Following the work principle and analysis results of this high speed and high accurate image sensors with light-section method in chapter 2, in this section we will deeply look into the existing evaluation method of this image sensor, by analyzing the problems of the existing evaluation method. we try to find out a method by which we can comprehensively evaluation this image sensor especially for the evaluation of background light suppression characteristics and range finding accuracy.

3.1.1 Problems of Existing Evaluation Method

In this work, although the existing evaluation results shows : a row-parallel frame access architecture has been proposed for the high-speed range finding and the row-parallel search operations are executed by a chained search circuit embedded in a pixel on the focal plane, the bit-streamed column address flow enables row-parallel address acquisition with a compact circuit implementation. Moreover a multi-sampling technique is available for range accuracy improvement. A 375 x 365 3-D range-finding image sensor has been designed and fabricated in a one-poly five-metal (1P5M) 0.18- m standard CMOS process. It attains a high-speed frame access rate with multiple samplings. The maximum frame access rate is 394.5 kHz with four samplings, which has a potential capability of 1052 range maps/s in the case of a sufficiently strong beam intensity. Then it provides 1.10 mm range accuracy at a target distance of 600 mm. It has been improved up to 0.2 sub-pixel resolution by the multi-sampling technique. Actually because this image sensor used a typical and convention light-section method and a common pixel circuit, as we discussed in chapter 2, background light is quite a issue which can affect the performance of the image sensor, but in the existing evaluation method, background light suppression characteristic is not evaluated. For this work to evaluate the background light suppression characteristic, the the following issues should be evaluated as well.

- Signal-to-Background Ratio which stands for the sensitivity of light detection.
- Range of signal sight intensity in some level of background light while the range information can be derived.
- Range of background light intensity in some level of signal light while the range information can be derived.
- Range of background light and signal light intensity while the range information can

be derived.

- Other issues which could affect the range information can be derived.

About the rang finding accuracy, in the existing evaluation method, the measurement results only shows the relation of real distance and range accuracy. This work have a 2.78cm (0.5sub-pixel) resolution while the distance between the target object and the image sensor is 600mm without multi-sampling and a range Accuracy of 0.11cm (0.2sub-pixel) resolution at the same distance ,with 4 times sampling. But the results did not show the typical issues as background light suppression characteristics which could affect the range find accuracy, the following issues are still needed to be evaluated.

- Range accuracy with signal light intensity.
- Range accuracy with background Light Intensity.
- Range accuracy with signal light intensity and background light intensity.

3.1.2 Evaluation of Background Light Suppression Characteristic and Range Finding Accuracy

Towards the problems of existing evaluation method which we listed up in section. 3.1.1 and base on the numerical analysis of this sensor, we present a numerical evaluation method for background light suppression characteristic and range finding accuracy in this section. As we analyzed in chapter 2, the voltage caused by photodiode V_{pd} can be calculated by photo-current I_{pd} which include two components I_{sig} induced by the signal light and I_{bg} induced by background light,well capacity C_{pd} and integration time t.

$$V_{pd} = \frac{I_{pd} * t}{C_{pd}} = \frac{(I_{sig} + I_{bg}) * t}{C_{pd}} \tag{3.1}$$

Here, the output voltage can be divided into V_{sig}, V_{bg} and V_{noise} corresponding to the signal light, background light and another noises respectively.

$$V_{pd} = V_{sig} + V_{bg} + V_{noise} \tag{3.2}$$

By assuming the value of I_{sig} and I_{bg}, V_{sig} and V_{bg} can be easily calculated. The signal intensity can be detected in the condition

$$V_{sig} + V_{bg} + V_{noise} \leq V_{sat} \tag{3.3}$$

And, take the gain of the source follower in consider, the output voltage V_{out} after amplified is given by

$$V_{out} = A_{sf} * (V_{sig} + V_{bg} + V_{noise}) \tag{3.4}$$

The pixel is activated when V_{out} is higher then the threshold voltage V_{cmp}.

$$V_{out} \geq V_{cmp} \tag{3.5}$$

In this system, a laser pulse is used as a light source, so we can assume this optical pulse as a Gaussian shape. V_i is the voltage value at the location i, x_{real_peak} is the real peak location on the sensor plane and σ characterizes the pulse width. σ is assumed to 0.45FWHM.

$$V_i = V_{sig} * e^{\frac{-\left(x_i - x_{real\_peak}\right)^2}{2*\sigma^2}} \tag{3.6}$$

Then, to find out how the resolution of AD converter affect the background light suppression and range resolution, V_{sig} is the input of the AD converter, and the output of AD converter can be calculated using resolution ΔV_{ADC} and integral function. Normally the input of AD converter are represented by this relation. Fig.**??** shows the calculation results by using this results, as we see in the figure the error will become smaller when we are using a high resolution AD converter.

$$V_{pix} = \left[\frac{V_i}{\Delta V_{ADC}}\right] * \Delta V_{ADC} \tag{3.7}$$

to determine the value of peak x_{cal_peak}, x_{cal_peak} may be estimated by using the centroid algorithm

$$x_{cal\_peak} = \frac{\sum_{i=1}^{N} V_{pix} * x_i}{\sum_{i=1}^{N} x_i} \tag{3.8}$$

by substitute 3.7 and 3.6 into 3.8, the x_{cal_peak} can be calculated by

$$x_{cal\_peak} = \frac{\sum_{i=1}^{N} \left[\frac{V_{sig} * e^{\frac{-\left(x_i - x_{real\_peak}\right)^2}{2*\sigma^2}}}{\Delta V_{ADC}} \right] * \Delta V_{ADC} * x_i}{\sum_{i=1}^{N} x_i} \tag{3.9}$$

Finally, to evaluate the accuracy of peak detection, we use the function give by

$$\Delta x_{peak} = |x_{cal\_peak} - x_{real\_peak}| \tag{3.10}$$

We use Signal-to-Background Ratio'(SBR') to evaluate the sensitivity of the image sensor. SBR' is given by

$$SBR' = 20 \log \frac{V_{sig\_min}}{V_{bg}} = 20 \log \frac{\Delta V_{ADC} + V_{bg}}{V_{bg}} \tag{3.11}$$

As, shown in Fig.**??**, the incident light is a Gaussian Shape Signal on the sensor, let put a 1 x 10 pixel on the x-axis as shown in the Figure, when we are using a 2-bit AD converter, after digitalizing, we can get a figure as shown in Fig. 3.2 Fig. 3.3 shows the evaluation results of this sensor, one area was determined by SBR', signal light intensity and background light intensity. In this area, the range information can be acquired by this image sensor and we can calculated the range accuracy by the method we present.Upon this area, after the pixel itself is saturated although the pixel is activated, and the range information we still can acquired, we can not control the range accuracy because we can on get a voltage of signal as V_{sat}. The maximum signal light intensity is determined by V_{sat}, V_{bg} and V_{noise}. As shown in Fig. 3.3 if the signal light can only be detected when it's intensity is stronger than the background light intensity. For a fixed signal light intensity, when the intensity of background light is getting stronger, SBR' becomes low. In Fig. 3.4, We can find out that one area was determined by range accuracy, signal light intensity and background light intensity. This area shows the range of range finding accuracy while using the signal light and the background light we assumed in this evaluation. Fig. 3.4 shows that the range accuracy will get worse when the background level increases, and for a fixed background level, the stronger signal light level can acquire a higher range accuracy.

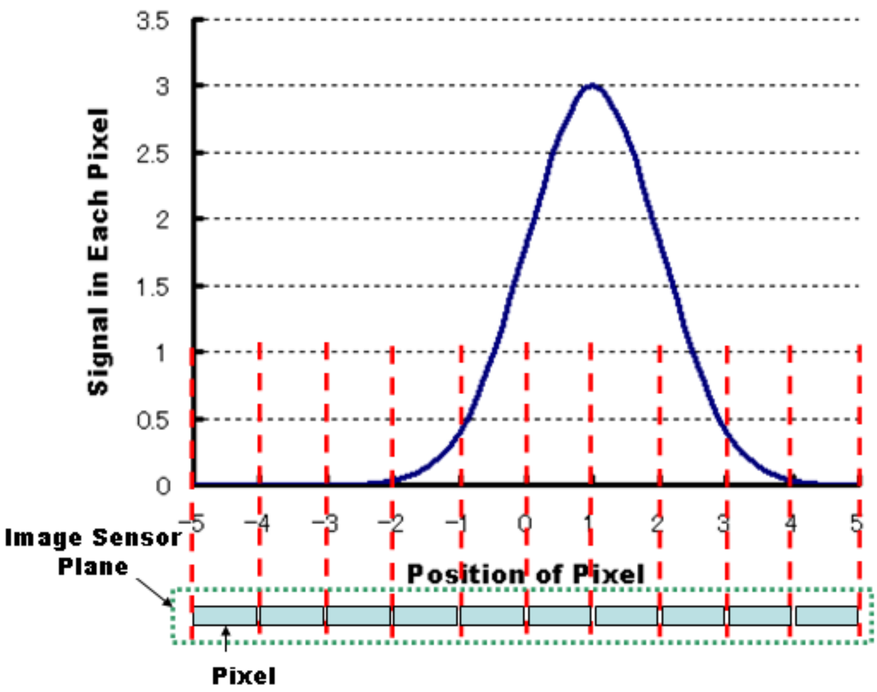

Figure 3.1 Light Signal on Plane of Image Sensor

Table 3.1 Parameters for the evaluation of [31]

Parameter	Value/Range
Integration Time	50μs
σ	0.45FWHM
Well Capacity	40fF
A_{sf}	1
ADC/TDC	1bit
Distance	1100mm

3.1.3 Summary

A evaluation method of background light suppression characteristics and range finding accuracy for this high speed and high accurate image sensors with light-section method has been presented in this section. Using this method the issues which listed up in the existing evaluation method as the background light suppression characteristics and range finding accuracy of this sensor have been evaluated successfully. For the background light suppression characteristics:

- Signal-to-Background Ratio' is successfully evaluated. This sensor has a 20.83dB

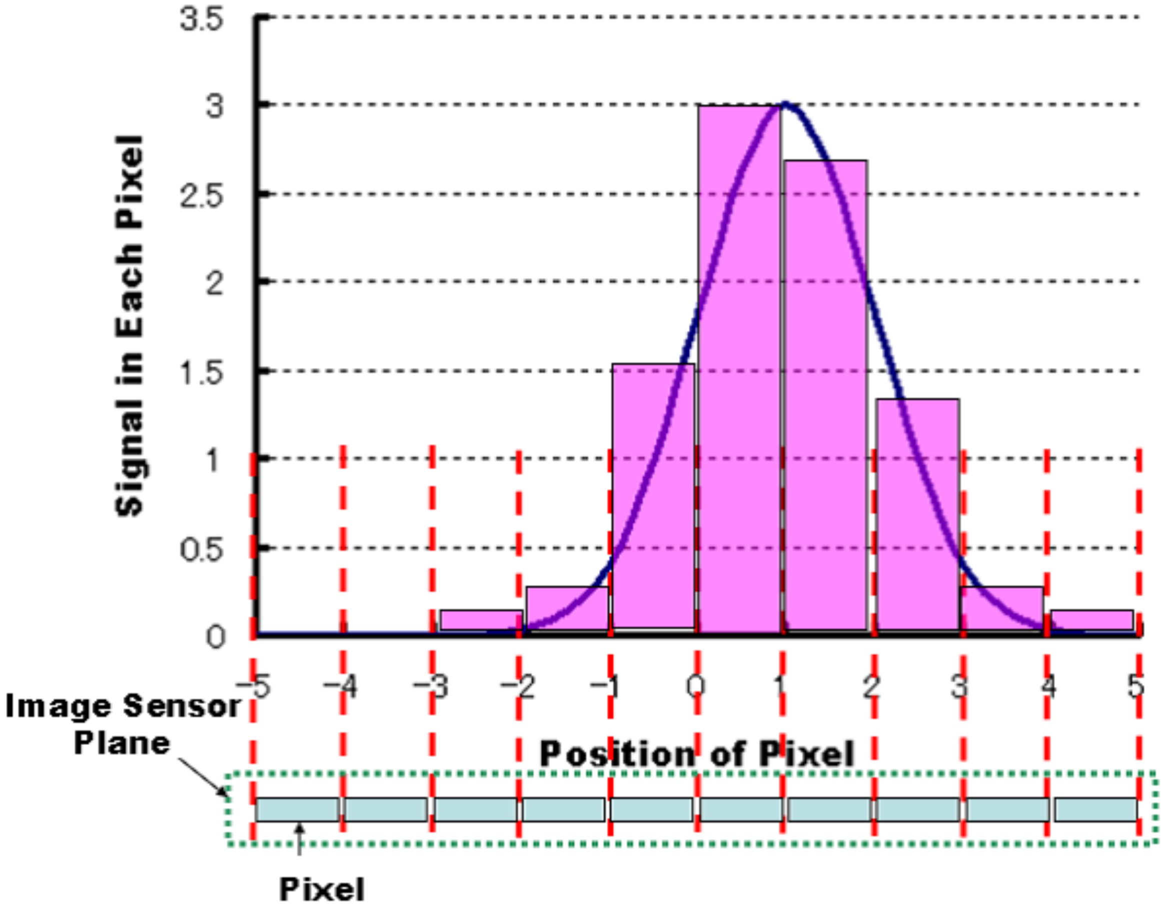

Figure 3.2 Calculated Light Signal on Plane of Image Sensor while using 2-bit ADC

SBR' while the signal intensity equates to 0.01V and the background light equates to 0.001V. While the signal intensity equates to 1.5V and the background light equates to 0.24V, the sensor has a 0.06dB SBR'.

- Range of signal light intensity in some level of background light while the range information can be derived is successfully evaluated. The range of incident signal light is 0.01V $\sim$ 1.5V while the background intensity equates to 0.001V.
- Range of background light intensity in some level of signal light while the range information can be derived is successfully evaluated. The signal light of 1.5V can be detected by this sensor while the range of background light is 0.001V $\sim$ 0.241V.

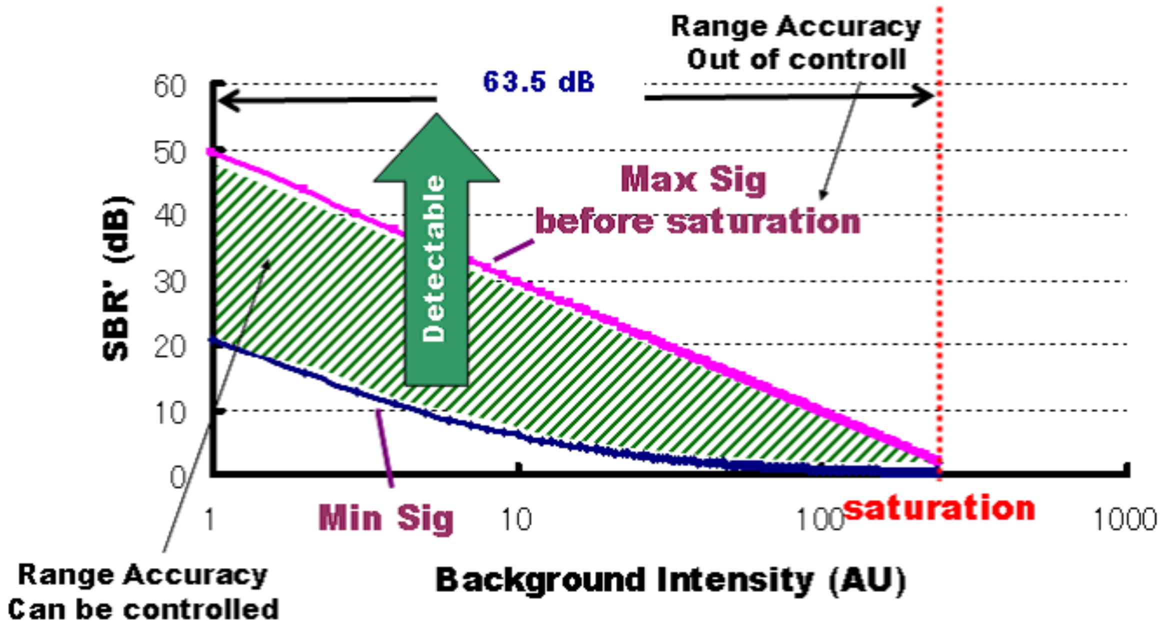

Figure 3.3 Range Information Detectable Area determined by Signal Light and Background Light for LS conventional

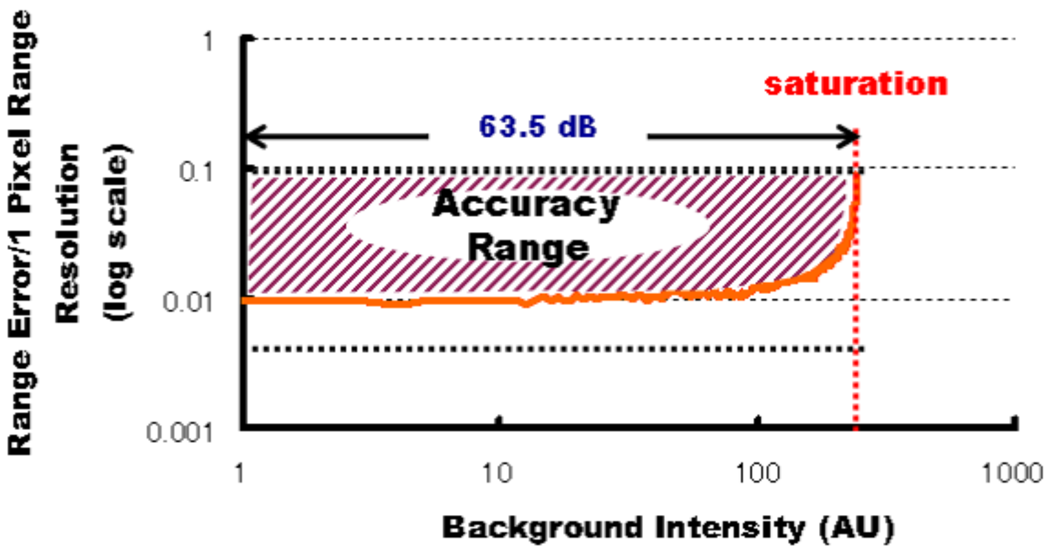

Figure 3.4 Range Accuracy Area determined by Signal Light and Background Light for LS conventional

- Range of background light intensity and signal Intensity while the range information can be derived is successfully evaluated. The range information can be acquired by this sensor while the range of background light is 63.5dB, and the range of incident signal light is 43.5dB.

The range accuracy was also evaluated under the consideration of the background light issue. The evaluation results shows:

- range accuracy with signal light intensity and background light intensity is successfully evaluated. The accuracy acquired by this sensor is 0.004 pixel pitch $\sim$ 0.089 pixel pitch while the range of background light is 63.5dB, and the range of incident signal light is 43.5dB.

3.2 Evaluation of High Dynamic Range and High Background Light Suppression Image Sensors with Light-Section Method

Compare with the sensor we evaluated in section. 3.1.2, although this high dynamic range and high background light suppression image sensor also uses the light-section method, for the detection of the signal light with a weak intensity in strong background light, the light-section principle evolute to a light-section based demodulated method as we introduced in section. 2.2. As we have numerically analyzed the work principle and pixel circuit in chapter 2, in this section we will deeply look into the existing evaluation method of this image sensor, by analyzing the problems of the existing evaluation method. we try to find out a method by which we can comprehensively evaluation this image sensor especially for the evaluation of background light suppression characteristics and range finding accuracy.

3.2.1 Problems of Existing Evaluation Method

Using the existing evaluation method ,this work has the capability of sensitive and selective light detection in wide dynamic range to utilize a low light levels that is safe for human eyes in a nonuniform contrast target scene. The present sensor achieves highly sensitive light detection of -18-dB SBR in 48-dB background illumination. It also realizes high selectivity to detect only a target projected light in other ambient lights due to -13-dB suppression to even harmonics of a correlation frequency. It has a trade off between sensitivity and frame rate, however, its possible frame rate is 2000 fps at -16-dB SBR. In the range finding system, the maximum error of range data is 1.5 mm at a distance of 1000 mm. For the evaluation for background light suppression characteristics, this work show the Signal-to-Background Ratio ¡-18 dB in a range of 48dB background light while the background light intensity is limited by the test equipment. These are not enough to show the background light suppression characteristics of this sensor comprehensively. For the comprehensively evaluation of background light suppression characteristics the following items are need to be evaluated.

- Range of signal light intensity in some level of background light intensity in which the range information can be derived is needed to be evaluated.
- Range of background light intensity in some level of signal light in which the range information can be derived is needed to be evaluated.
- Range of background light intensity and signal Intensity in which the range information can be derived is needed to be evaluated.
- Other issues which could affect the range information is needed to be evaluated. (In this case, the gain of current mirror should be evaluated, because the effect of SBR')

The evaluation results acquired by using the existing evaluation method, only shows the relation of real distance and range accuracy. This work has a accuracy of 3.2mm (max error) and 0.89mm (std) at the full area, 1.5mm (max error) and 0.6mm (std) at the effect area while the distance between the target object and the image sensor is 1000mm $\sim$ 1100mm. But the results did not show the typical issues as background light suppression characteristics which could affect the range find accuracy, the following issues are still needed to be evaluated.

- Range accuracy with signal light intensity.
- Range accuracy with background light intensity.
- Range accuracy with signal light intensity and background light intensity.
- Range accuracy with numbers of detection.

3.2.2 Evaluation of Background Light Suppression Characteristic and Range Finding Accuracy

Towards the problems of existing evaluation method which we listed up in section. 3.2.1 and base on the numerical analysis of this sensor, we present a numerical evaluation method for background light suppression characteristic and range finding accuracy in this section. As we analyzed in chapter 2, the current induced by photodiode is given by

$$I_{pd} = I_{dc} + I_{ac} \tag{3.12}$$

The low-pass filter generates the average current, αI_{avg}, as follows.αI_{avg}

$$\alpha I_{avg} = \alpha \overline{I_{pd}} = \alpha \left(I_{dc} + \overline{I_{ac}} \right) \tag{3.13}$$

In our evaluation, we assume α as 4.

The constant current, I_{dc}, is adaptively suppressed by the current-mode suppression circuit. Here, a time constant of the low-pass filter is designed at 1.2 ms in a typical situation. It can be adjusted by the external bias voltage, V_r. The output current, I_{mod}, of the suppression circuit is given by

$$I_{mod} = \alpha^{'} I_{dc} - \alpha I_{avg} \approx \alpha \left(I_{ac} - \overline{I_{ac}} \right) \tag{3.14}$$

The output current, I_{mod}, is converted to a voltage level of V_{mod} by a logarithmic-response circuit.

$$V_{mod} = \beta \log \left(I_{offset} + I_{mod} \right) \tag{3.15}$$

$$V_{out+} - V_{out-} \geq V_{cmp} \tag{3.16}$$

By combing all the process we discussed before, the final output of the pixel can be given by

$$V_{out} = \sum_{i=1}^{N} \left(V_{out+} - V_{out-} \right) = \sum_{i=1}^{N} \beta \int_{t-T}^{t} \log I_{PD} \left(\tau \right) \Delta V_{MPY} \left(\tau \right) d\tau \tag{3.17}$$

In this system, a laser pulse is used as a light source, so we can assume this optical pulse as a Gaussian shape. V_i is the voltage value at the location i, x_{real_peak} is the real peak location on the sensor plane and σ characterizes the pulse width. We assume σ as 0.45FWHM.

$$V_i = V_{sig} * e^{\frac{-\left(x_i - x_{real\_peak}\right)^2}{2*\sigma^2}} \tag{3.18}$$

As we discussed in section. 2.1, the resolution of AD converter is quite a factor which will affect the range finding accuracy. So as a input to AD converter V_{out}, with the consideration of resolution of AD converter ΔV_{ADC}, the output of converter V_{pix} is given by

$$V_{pix} = \left[\frac{V_i}{\Delta V_{ADC}}\right] * \Delta V_{ADC} \tag{3.19}$$

to determine the value of peak x_{cal_peak}, x_{cal_peak} may be estimated by using the centroid algorithm

$$x_{cal\_peak} = \frac{\sum_{i=1}^{N} V_{pix} * x_i}{\sum_{i=1}^{N} x_i} \tag{3.20}$$

by substitute 3.19 and 3.18 into 3.20, the x_{cal_peak} can be calculated by

$$x_{cal\_peak} = \frac{\sum_{i=1}^{N} \left[\frac{V_{sig} * e^{\frac{-\left(x_i - x_{real\_peak}\right)^2}{2*\sigma^2}}}{\Delta V_{ADC}}\right] * \Delta V_{ADC} * x_i}{\sum_{i=1}^{N} x_i} \tag{3.21}$$

Finally, to evaluate the accuracy of peak detection, we use the function give by

$$\Delta x_{peak} = |x_{cal\_peak} - x_{real\_peak}| \tag{3.22}$$

We use Signal-to-Background Ratio'(SBR') to evaluate the sensitivity of the image sensor. SBR' is given by

$$SBR' = 20 \log \frac{V_{sig\_min}}{V_{bg}} = 20 \log \frac{\Delta V_{ADC}}{V_{bg}} \tag{3.23}$$

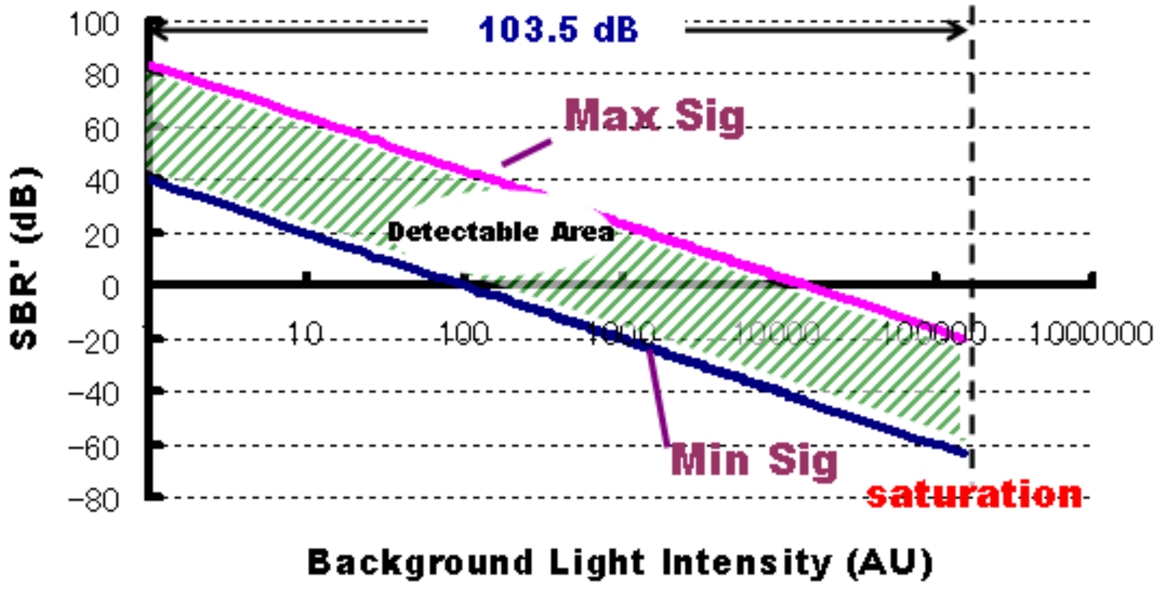

Figure 3.5 Range Information Detectable Area determined by Signal Light and Background Light for LS Demodulation

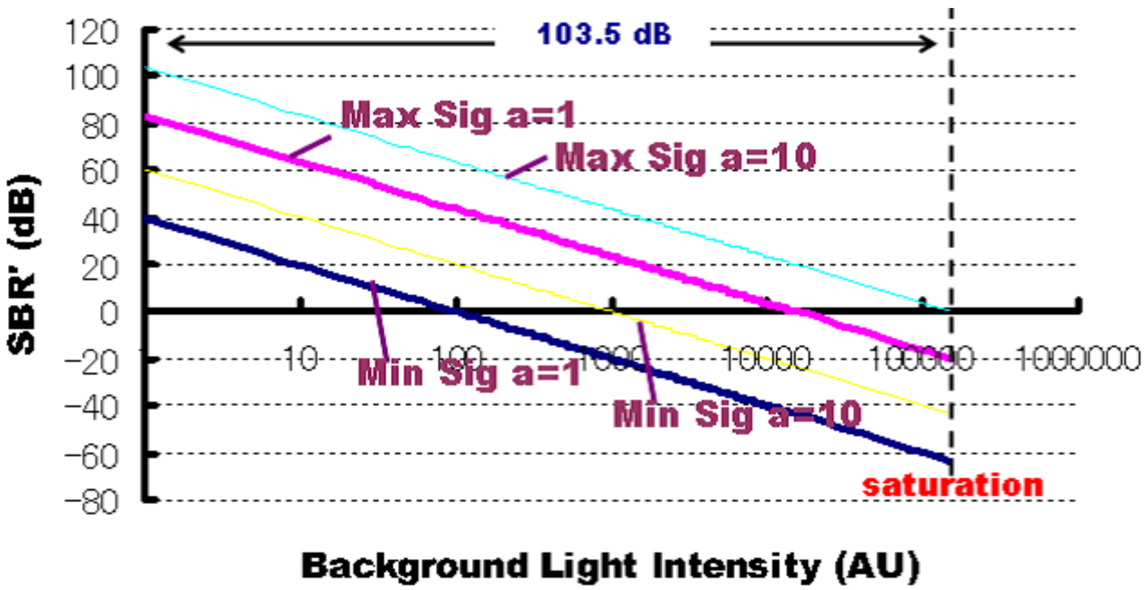

Figure 3.6 Range Accuracy Area determined by Signal Light and Background Light for LS Demodulation while the gain of current mirror is 1 and 10

Fig. 3.5 shows the evaluation results of this sensor, one area was determined by SBR', signal light intensity and background light intensity. In this area, the range information can

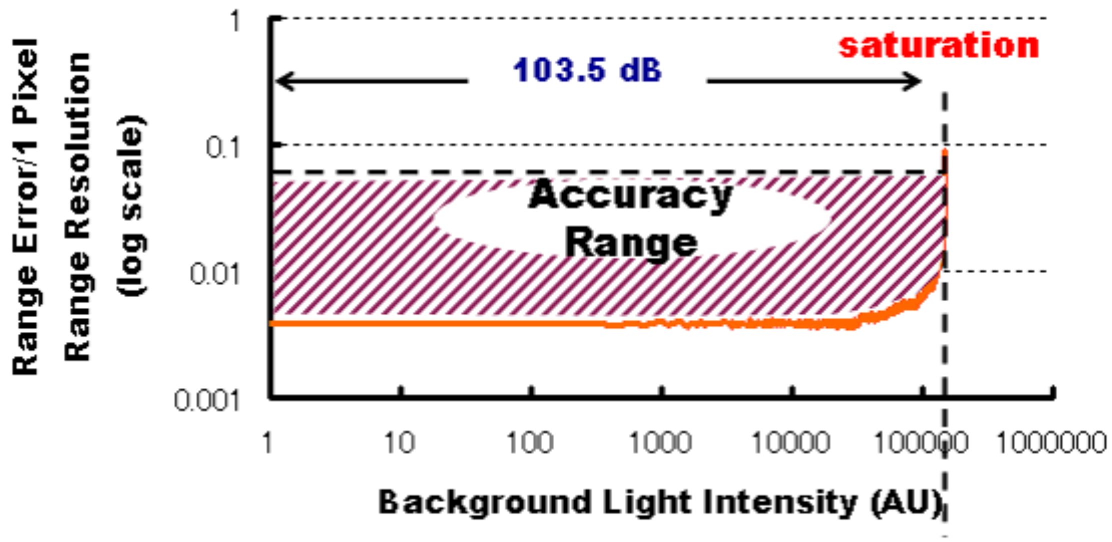

Figure 3.7 Range Accuracy Area determined by Signal Light and Background Light for LS Demodulation

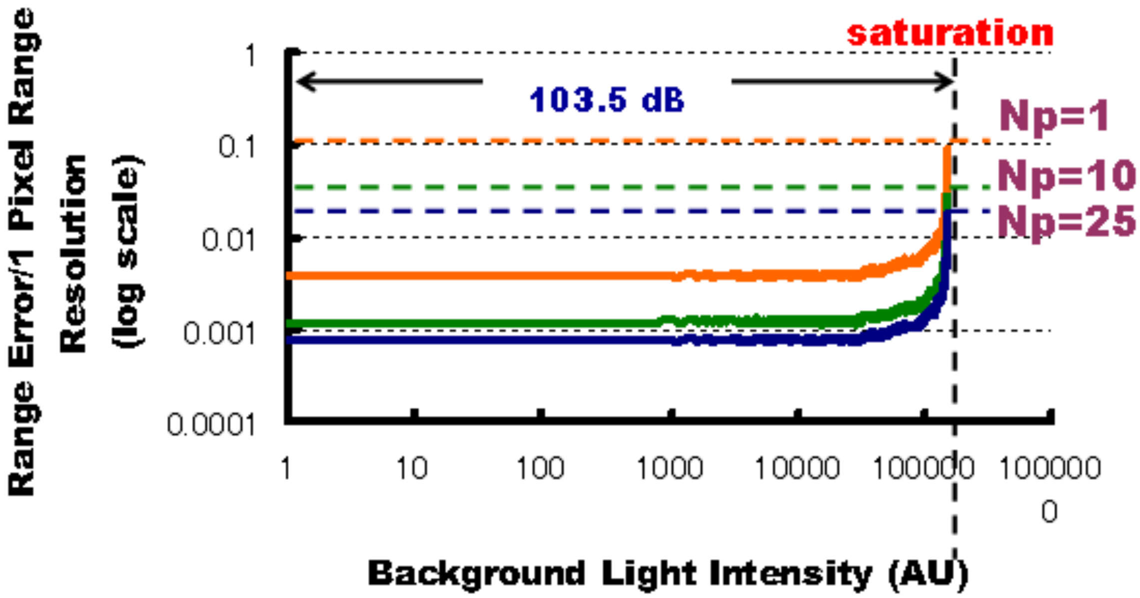

Figure 3.8 Range Accuracy Area determined by Signal Light and Background Light for LS Demodulation while the Numbers of Averaging is 1, 10, and 25(Numbers of frame)

be acquired by this image sensor. The maximum signal light intensity is determined by V_{sat}, and V_{dc}. As shown in Fig.?? even the signal light can is weaker than the background level the

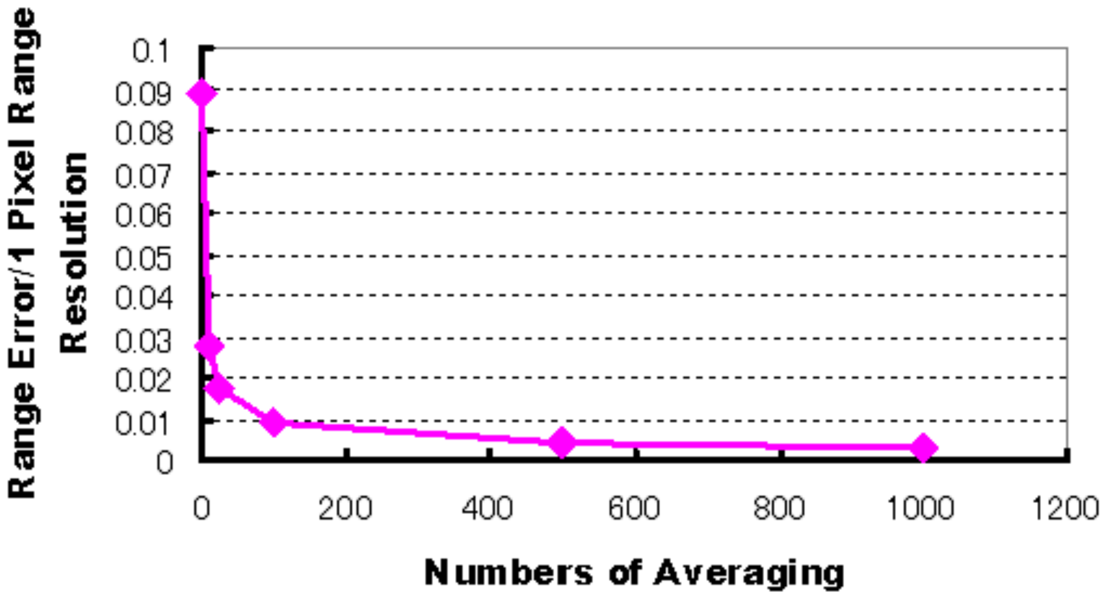

Figure 3.9 Range Accuracy of this sensor with Times of Detection for LS Demodulation

signal light still can be detect by using the background light suppression technology and the demodulation principle. In Fig.**??**, the evaluation results shows that the gain of the current mirror which was used in this work, affect the SBR' extremely. The bigger the gain is, the higher the SBR' will be. In Fig. 3.7, we can find out that one area was determined by range accuracy, signal light intensity and background light intensity. This area shows the range of range finding accuracy while using the signal light and the background light we assumed in this evaluation. Fig. 3.4 shows that the range accuracy will get worse when the background level increases, and for a fixed background level, the stronger signal light level can acquire a higher range accuracy. Fig. 3.8 shows the evaluation result while using the average technology, N_p is the frame number in this figure. We can understand from this figure that the range accuracy gets lower by a factor of $N_p^{1/2}$. Fig. 3.9 shows the evaluation result while increasing the detection times for the signal light, as shown in the figure, the range accuracy also gets lower while increasing the detection times, but is limited by anther noises as thermal noise and readout noise.

Table 3.2 Parameters for the evaluation of [27]

Parameter	Value/Range
Integration Time	50μs
σ	0.45FWHM
α	1,10
β	1
Well Capacity	C_1=C_2=37fF
ADC/TDC	1bit
Distance	800-1200mm

3.2.3 Summary

We presented a comprehensively evaluation method of background light suppression characteristics and range finding accuracy for high dynamic range and high background light suppression image sensor also uses the light-section method in this section. Using this method the issues which listed up in the existing evaluation method as the background light suppression characteristics and range finding accuracy of this sensor have been evaluated successfully. For the background light suppression characteristics:

- Range of signal light intensity in some level of background light while the range information can be derived is successfully evaluated.
- Range of background light Intensity in some level of signal light while the range information can be derived is successfully evaluated.
- Range of background light and signal Intensity while the range information can be derived is successfully evaluated. The range information can be acquired in 103.5dB background light intensity range, and the range of signal light intensity is 43.5dB.
- Gain of current mirror which will affect the SBR' of the image sensor is also successfully evaluated.

We also evaluated the range finding accuracy under the consideration of the background light issue. The evaluation results shows:

- The relation among range accuracy, signal light intensity and background light is successfully evaluated. The accuracy is 0.004 pixel pitch $\sim$ 0.089 pixel pitch in a 63.5dB background light intensity Range, with a 43.5dB signal light intensity range.

- Relation between Range Accuracy and Numbers of Averaging is successfully evaluated.

Chapter 4

Evaluation of Background Light Suppression Characteristic and Range Finding Accuracy for TOF Method

After we discussed the existing problems of the existing evaluation and presented our evaluation method to evaluate the two light-section image sensors:a high Speed and high accurate image sensors with light-section method, a high dynamic range and high background light suppression image sensors with light-section method in chapter 3, In this chapter we will discuss the time-of-flight image sensors. As the same, we also take two typical types of time-of-flight image sensors: a Time-of-Flight image sensor with lock-in pixel structure and a Time-of-Flight image sensor with single-photon avalanche diodes as our base. Nevertheless these two image sensors have been evaluated in their works respectively, but for the evaluation of background light characteristics and range finding accuracy. The evaluations are not enough. In this chapter we will discuss the problems of the existing evaluation for them respectively, and towards the problems we will present our method to solve the existing problems and provide a new respect to evaluate the image sensors for 3-D measurement.

4.1 Evaluation of Time-of-Flight Image Sensor with Lock-in Pixel Structure

Compare with light-section method, time-of-flight method is weaker to background light. For the detection of the signal light with a weak intensity in strong background light, the demodulated method are commonly used by time-of-flight image sensors. As we have numerically analyzed the work principle and pixel circuit in chapter 2, one can use the lock-in structure to realize the demodulate process, in this section we will deeply look into the existing evaluation method of this image sensor, by analyzing the problems of the existing evaluation method. we try to find out a method by which we can comprehensively evaluation this image sensor especially for the evaluation of background light suppression characteristics and range finding accuracy.

4.1.1 Problems of Existing Evaluation Method

In this work, although the existing evaluation results shows : the best range resolution measured in this is 2.35 cm with light pulsewidth of 100 ns at 30 fps and could be improved using a shorter light pulsewidth or by a factor of $N^{1/2}$ by averaging N frames of images. Also, the background light is taken into consider to calculate the range accuracy in functions, but in the existing evaluation method, background light suppression characteristic is not evaluated. For this work to evaluate the background light suppression characteristic, the the following issues should be evaluated as well.

- Signal-to-Background Ratio which stands for the sensitivity of light detection.
- Range of signal sight intensity in some level of background light while the range information can be derived.
- Range of background light intensity in some level of signal light while the range information can be derived.
- Range of background light and signal light intensity while the range information can be derived.
- Other issues which could affect the range information can be derived.

About the rang finding accuracy, in the existing evaluation method, the measurement results only shows the relation of range accuracy and time delay and the relation of range accuracy with signal light intensity, and relation with numbers of averaging, relation of range accuracy, signal intensity and pulse width of laser light source. when the time delay is 1ns, the signal light intensity equates to 0.7V the range accuracy is 2.9cm, the range accuracy will reduce to 3.45cm while the time delay is 50ns and the signal light intensity is 0.7V, furthermore, the range accuracy will get back to 2.9 cm again while the the time delay change to 100ns and the signal light intensity is 0.7V. At the distance 1m under the signal intensity equates to 1.4V and without averaging, the range accuracy is 2.35cm. When using the averaging technology the range accuracy will promote form 7cm to 1.4cm when the no averaging and with 25 frames averaging using the 0.25V signal intensity. meanwhile, the range accuracy will promote form 2.4cm to 0.48cm when the no averaging and with 25 frames averaging using the 1.3V. At the same time, when using a 10ns plusewidth and 0.2V intensity laser source while averaging 10 frames, the range accuracy is 0.4cm. Compare with this when using a 40ns plusewidth, the range accuracy is 1.4cm, using a 100ns plusewidth, the range accuracy is 2.6cm. But the results did not show the typical issues as background light suppression characteristics which could affect the range find accuracy, the following issues are still needed to be evaluated.

- Range accuracy with signal light intensity.
- Range accuracy with background light intensity.
- Range accuracy with signal light intensity and background light intensity.
- Range accuracy with signal light intensity, background light intensity and numbers of averaging.

4.1.2 Evaluation of Background Light Suppression Characteristic and Range Finding Accuracy

Towards the problems of existing evaluation method which we listed up in section. 4.1.1 and base on the numerical analysis of this sensor, we present a numerical evaluation method for background light suppression characteristic and range finding accuracy in this section. As we analyzed in chapter 2, the output of node N_1 and N_2 is given by

$$N_1 = \frac{I_{PD}}{q}\left(T_0 - T_D\right) \tag{4.1}$$

and

$$N_2 = \frac{I_{PD}}{q}T_D \tag{4.2}$$

the photo current, I_{PD}, has two components of a constant current of I_{dc} by an Background light and an alternating current of I_{ac} by a modulated light.

$$I_{pd} = I_{dc} + I_{ac} \tag{4.3}$$

respectively. the TOF which directly corresponds to is written as

$$TOF = \frac{T_0 N_2}{N_1 + N_2} \tag{4.4}$$

and the measured range, L is given by

$$L = \frac{cT_0 N_2}{2\left(N_1 + N_2\right)} \tag{4.5}$$

where is c the speed of light. If the output node capacitances are equal, the number of electrons collected can be replaced by their corresponding voltage level and 4.1.2 can be rewritten as

$$L = \frac{cT_0 V_2}{2\left(V_1 + V_2\right)} \tag{4.6}$$

by the lock-in principle, V_1 is give by

$$V_1 = \frac{1}{N}\sum_{i=1}^{N}\left(\int_{t-T}^{t} I_{C1}\left(t\right)dt - \int_{t-T}^{t} I_{C2}\left(t\right)dt\right) = \frac{1}{N}\sum_{i=1}^{N}\rho\int_{t-T}^{t} I_{PD}\left(t\right)V\left(t\right)dt \tag{4.7}$$

also, V_2 is give by

$$V_2 = \frac{1}{N}\sum_{i=1}^{N}\left(\int_{t-T}^{t} I_{C1}\left(t\right)dt + \int_{t-T}^{t} I_{C2}\left(t\right)dt\right) = \frac{1}{N}\sum_{i=1}^{N}\int_{t-T}^{t} I_{PD}\left(t\right)dt \tag{4.8}$$

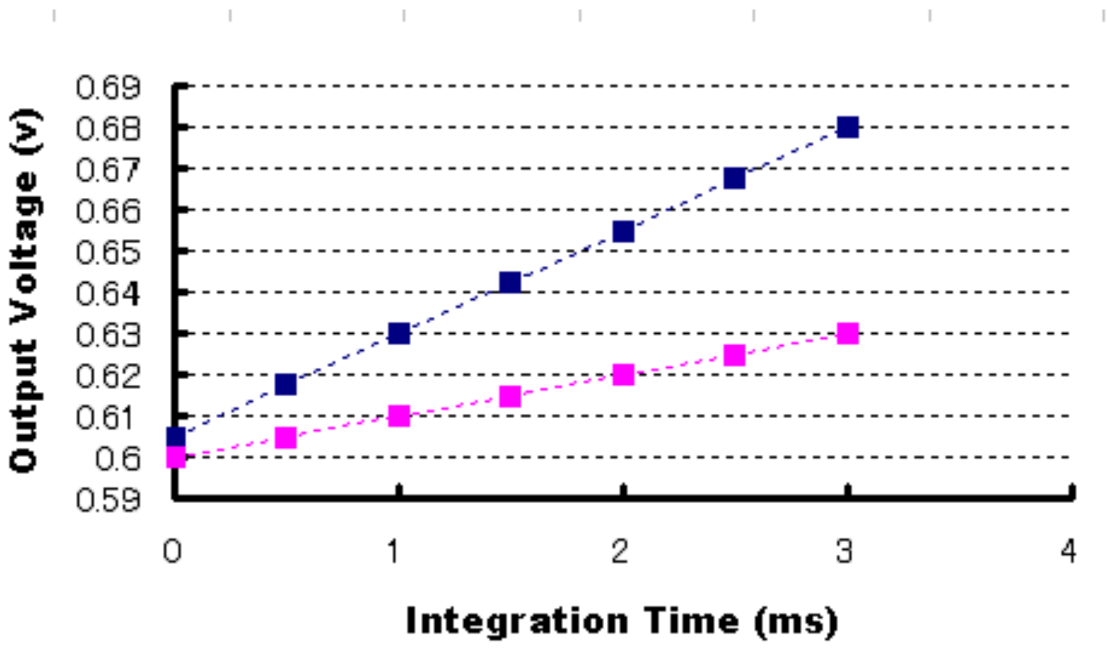

Figure 4.1 V1 and V2 with integration time

An offset voltage V_{offset}, caused by deep generated electrons diffusing to the surface and modifying the measured signal voltage, must be taken into consider while we are calculating the range L, with the consideration of the resolution of AD converter ΔV_{ADC},so L is give by

$$L_{cal} = \frac{cT_0\left(\left[\frac{V_2}{\Delta V_{ADC}}\right] * \Delta V_{ADC} - V_{offset}\right)}{2\left(\left[\frac{V_1}{\Delta V_{ADC}}\right] * \Delta V_{ADC} + \left[\frac{V_2}{\Delta V_{ADC}}\right] * \Delta V_{ADC} - 2V_{offset}\right)} \tag{4.9}$$

To evaluate the range finding accuracy, we use the function give by

$$\Delta L_{peak} = |L_{cal\_peak} - L_{real\_peak}| \tag{4.10}$$

We use Signal-to-Background Ratio'(SBR') to evaluate the sensitivity of the image sensor. SBR' is given by

$$SBR' = 20\log\frac{V_{sig\_min}}{V_{bg}} = 20\log\frac{\Delta V_{ADC}}{V_{bg}} \tag{4.11}$$

Fig. 4.5 shows the evaluation results of this sensor, one area was determined by SBR', signal light intensity and background light intensity. In this area, the range information can be acquired by this image sensor. The maximum signal light intensity is determined by V_{sat}

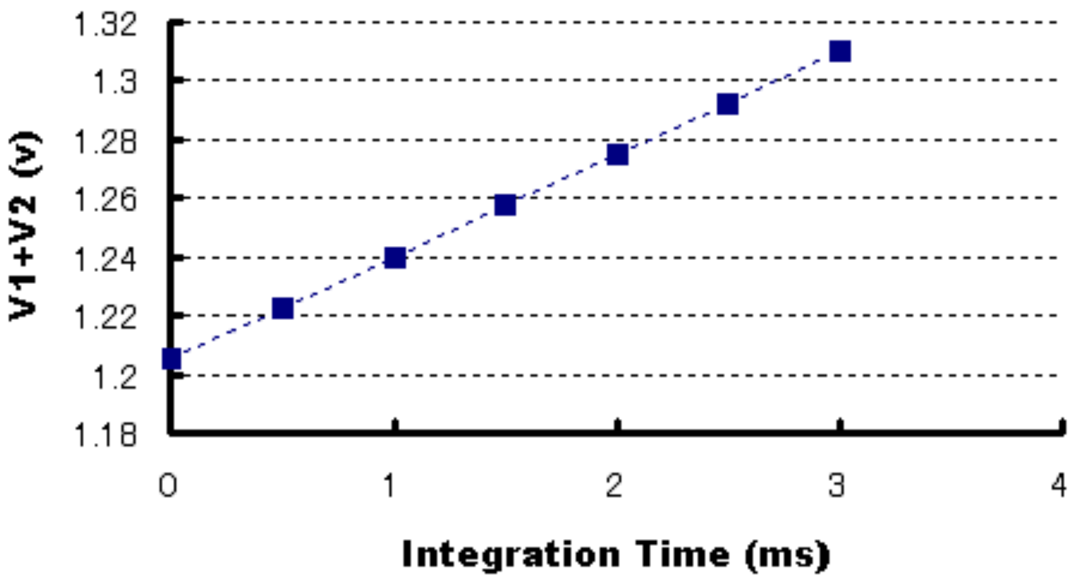

Figure 4.2 V1 + V2 with integration time

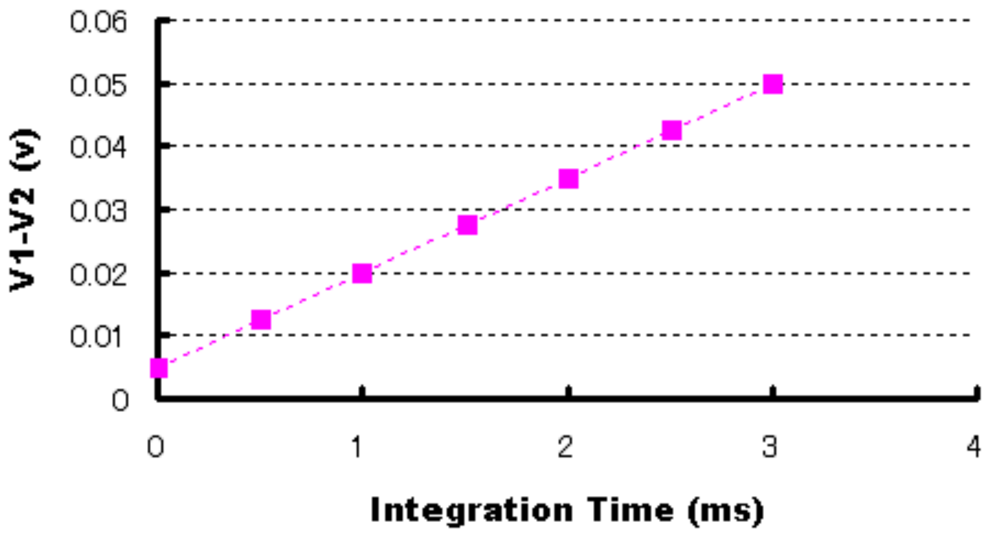

Figure 4.3 V1 - V2 with integration time

and V_{dc}. As shown in Fig. 4.5 even the signal light can is weaker than the background level the signal light still can be detect by using the background light suppression technology and the demodulation principle. In Fig. 4.6, we can find out that one area was determined by

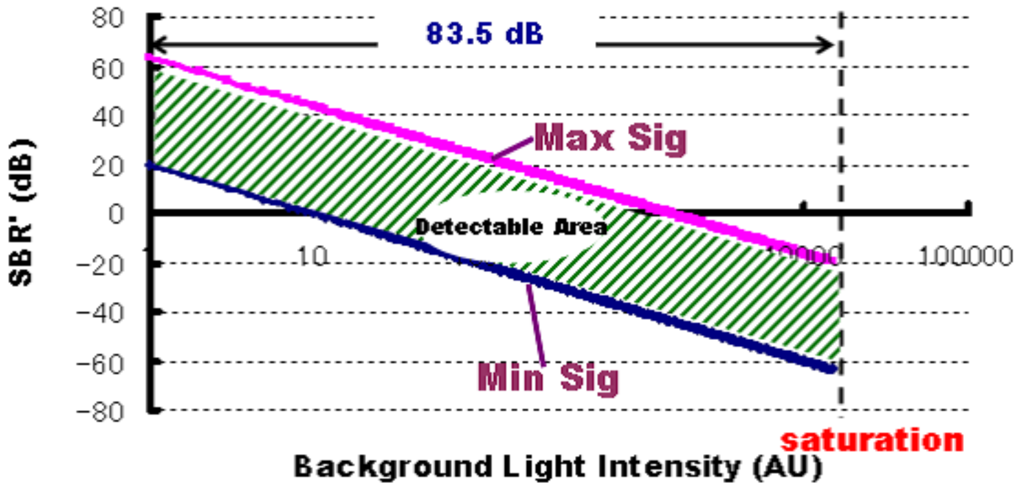

Figure 4.4 Range Information Detectable Area determined by Signal Light and Background Light for TOF-Lockin

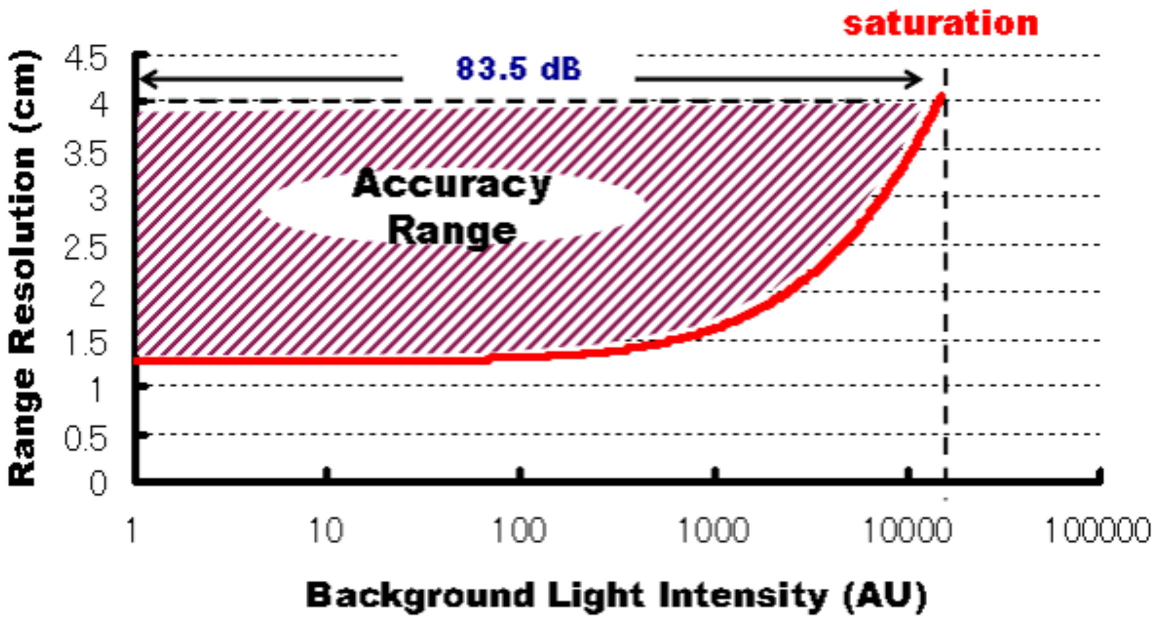

Figure 4.5 Range Accuracy Area determined by Signal Light and Background Light for TOF-Lockin

range accuracy, signal light intensity and background light intensity. This area shows the range of range finding accuracy while using the signal light and the background light we

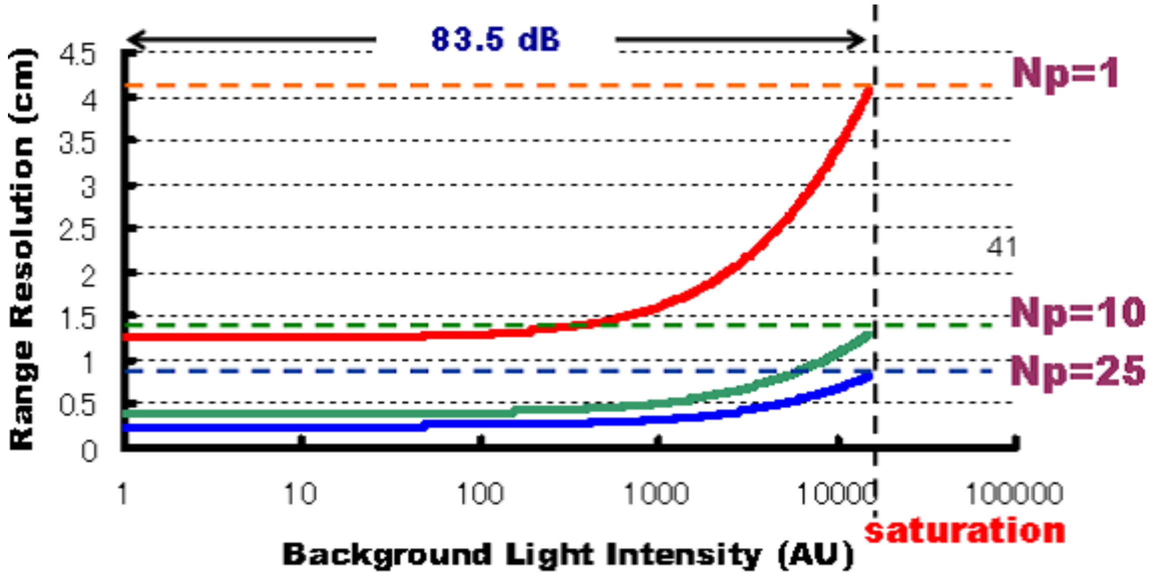

Figure 4.6 Range Accuracy Area determined by Signal Light and Background Light while the Numbers of Averaging is 1, 10, and 25(Numbers of frame) for TOF-Lockin

assumed in this evaluation. Fig. 4.6 shows that the range accuracy will get worse when the background level increases, and for a fixed background level, the stronger signal light level can acquire a higher range accuracy. Fig. 4.7 shows the evaluation result while using the average technology, N_p is the frame number in this figure. We can understand from this figure that the range accuracy gets lower by a factor of $N_p^{1/2}$.

Table 4.1 Parameters for the evaluation of [12]

Parameter	Value/Range
Integration Time	50μs
I_{ph}	0.01-1.5nas
τ	0.45FWHM
Well Capacity	C_1=C_2=10fF
ADC/TDC	1bit
Distance	800-12000mm

4.1.3 Summary

A evaluation method of background light suppression characteristics and range finding accuracy for this Time-of-Flight image sensor with lock-in pixel structure has been presented in this section. Using this method the issues which listed up in the existing evaluation method as the background light suppression characteristics and range finding accuracy of this sensor have been evaluated successfully. For the background light suppression characteristics:

- Range of signal light intensity in some level of background light in which the range information can be derived is successfully evaluated.
- Range of background light intensity in some level of signal light in which the range information can be derived is successfully evaluated.
- Range of background light and signal intensity in which the range information can be derived is successfully evaluated, while the range of background light intensity is 83.5dB, and the incident signal light intensity range is 43.5dB.

The range accuracy was also evaluated under the consideration of the background light issue. The evaluation results shows:

- The relation of range accuracy and signal light intensity and background light Intensity is successfully evaluated. The range accuracy is from 1.26 cm $\sim$ 4.07 cm while the range of background light intensity is 83.5dB, and the incident signal light intensity range is 43.5dB.
- The relation of range accuracy and signal light intensity and background light Intensity, numbers of averaging is successfully evaluated.

4.2 Evaluation of Time-of-Flight Image Sensor with Single-Photon Avalanche Diodes

The characteristics of Time-of-Flight image sensor with Single-Photon Avalanche Diodes were discussed in chapter 2, as we know, the range accuracy of this type of sensors is strongly depend on the background light suppression characteristics of the sensor. Commonly optical filters are used to help suppress the background light.

4.2.1 Problems of Existing Evaluation Method

Using the existing evaluation method, the accurate distance measurements were repeatedly achieved based on a short integration time of 50 ms even when signal photon count rates as low as a few hundred photons per second were available. The maximum nonlinearity.in distance measurement was 9 mm over the full measurement range. Time-varying uncertainty at the farthest distance was 5.2 mm. It also shows that the nonlinearity errors may be effectively improved with lower Time-to-Digital Converter nonlinearity and/or with parameterized nonlinearity compensation. No evaluation of background light suppression characteristics is done for this work, to evaluate the background light suppression characteristic, the following issues should be evaluated as well.

- Signal-to-Background Ratio which stands for the sensitivity of light detection.
- Range of signal sight intensity in some level of background light while the range information can be derived.
- Range of background light intensity in some level of signal light while the range information can be derived.
- Range of background light and signal light intensity while the range information can be derived.
- Other issues which could affect the range information can be derived.

For range find accuracy, the following issues are still needed to be evaluated.

- Range accuracy with signal light intensity.
- Range accuracy with background light intensity.
- Range accuracy with signal light intensity and background light intensity.
- Range accuracy with signal light intensity, background light intensity and numbers of averaging.

4.2.2 Evaluation of Background Light Suppression Characteristic and Range Finding Accuracy

Towards the problems of existing evaluation method which we listed up in section. **??** and base on the numerical analysis of this sensor, we present a numerical evaluation method for background light suppression characteristic and range finding accuracy in this section. As shown in Fig. 4.8, the probability of photon arriving of background Light, signal light, and the superimposing part is given by $P_n(t;E)$, $P_n(t;r(t))$, $P_n(t;s(t))$ respectively, All of these photons can induce a trigger, the probability of trigger caused by these photons is shown in Fig. 4.9. To calculate these probabilities, Firstly, we consider the background light. The probability of false trigger caused by background light is given by

$$P_n(t;E) = exp(-t * \eta_0 * E) \tag{4.12}$$

E is the arriving rate of the photons caused by the background light. Thus, the density of false trigger by background light is given by

$$\eta_0 * E \leq \tau^{-1} \tag{4.13}$$

Take the dead time t_{dead} of SPAD into consider. The probability of false trigger caused by background light is changed to

$$P_n(t;E) = exp(-min(t, t_{dead}) * \eta * E) \tag{4.14}$$

Also, the the density of false trigger by background light is changed into

$$\eta_0 * E \leq {t_{dead}}^{-1} \tag{4.15}$$

Firstly, we consider the Signal light. As a Gaussian shape signal, the signal return density can be give by,

$$r(t) = \frac{Q_r}{hv} * \frac{1}{\sqrt{2\pi} * \sigma} * exp(-t^2/2\sigma^2) \tag{4.16}$$

where the Q_r is the power of the signal, and σ is the pulse width. h is the Plank's constant.

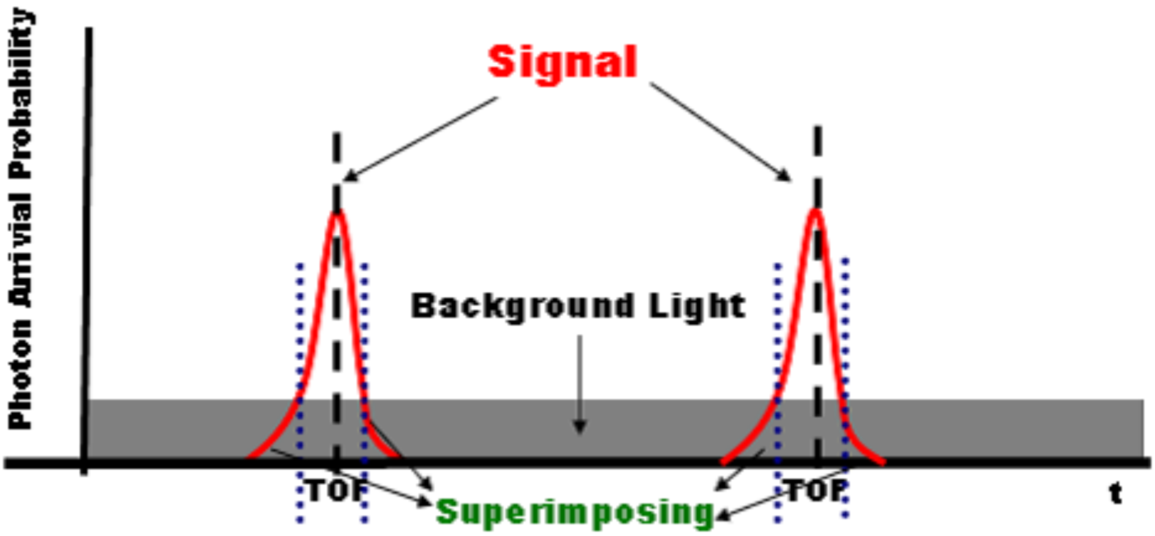

Figure 4.7 Probability of Arrived photons

Thus the signal return probability can be given as

$$P_n(t;r(t)) = exp\left(\frac{-1}{2} * \frac{\eta_0 * Q_r}{hv}\left[erf\left(\frac{t}{\sqrt{2} * \sigma}\right) + 1\right]\right) \tag{4.17}$$

So the totally probability of background light and signal light is given by

$$h(t) = P_n(t;E) + P_n(t;r(t)) + P_n(t;s(t)) \tag{4.18}$$

Take the resolution of time-of-digital converter into consider. The time-of-flight is acquired by calculating the arriving time centroid of the light by

$$TOF = \frac{\sum_{i=TOF'-PW/2}^{TOF'+PW/2} h(i\Delta t) * i\Delta t}{\sum_{i=TOF'-PW/2}^{TOF'+PW/2} h(i\Delta t)} \tag{4.19}$$

The resolution(LSB) of time-to-digital converter is assumed to 200ps. Both the signal and background light is evaluated by using the count rate of them.

4.2.3 summary

Because $P_n(t;s(t))$ is still under analyzing, in the future, we will summarize the results after the analysis is finished.

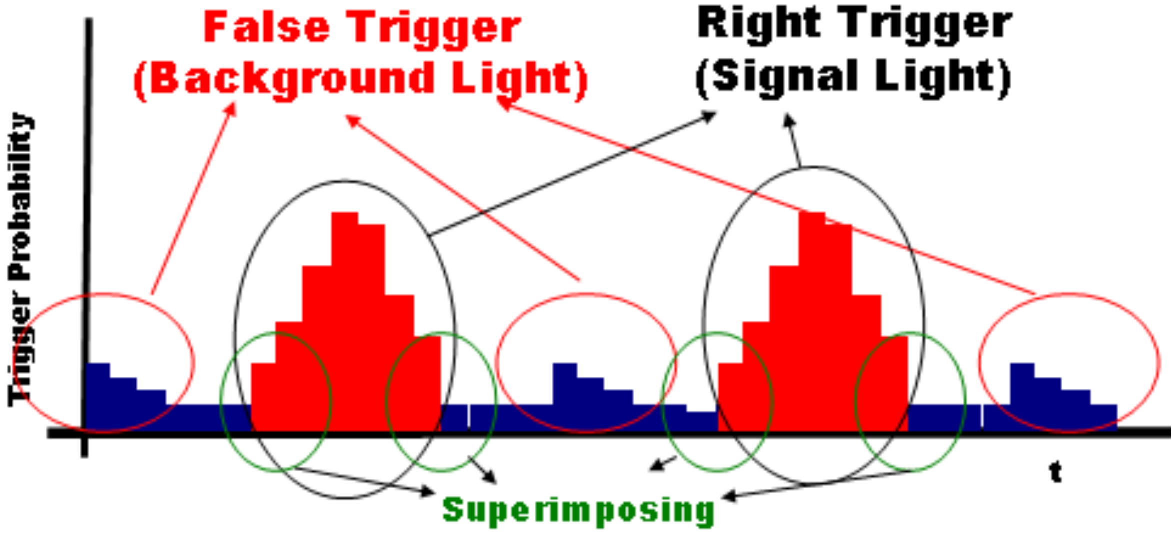

Figure 4.8 Probability of triggers cause by Arrived photons

Table 4.2 Parameters for the evaluation of [11]

Parameter	Value/Range
Integration Time	50μs
σ	0.45FWHM
LSB(TDC)	90ns
Distance	800-50000mm

Chapter 5

Evaluation of Image Sensors base on Background Light Suppression Characteristic and Range Finding Accuracy

Base on the evaluation methods of background light suppression characteristics and range finding accuracy for 3-D measurement using smart image sensors with light-section and time-of-flight methods we presented in chapter 4 and chapter 5, As reference, in this chapter, we evaluated anther four 3-D measurement systems which are using smart image sensors as the key component of the system by our presented methods as well.

As we known, there are so many describing the performance of different sensors. However, incurring the risk of an incomplete comparison, some characteristic numbers are collected in Table I of different research works as well as already available products, also including the own results.

For the light-section, a real-time measurement system based on the light-section method consists of multiple range finders using the smart image sensors and beam projectors, and target objects are captured by the range finders from multiple directions [] is evaluated by our presented methods. Another sensor which is also based on light-section method can detect the laser light, even under very strong ambient-illumination levels by using a multiple-capture frame-correlated double sampling[] is also evaluated.For the time-of-flight, a image sensor based on multiple-pulse indirect Time-Of-Flight technique, wing to an differential pixel architecture, which allows for the detection of very short and low intensity light pulses []is also evaluated. A time-of-flight depth sensor which employing a correlation based concept[] is also evaluated. The evaluation results as we shown and compared in Table. 5.1,

Table 5.1 Evaluation Results Comparison

Parameter	[59]	[60]	[31]	[27]	[61]	[62]	[12]	[11]
Type	LS	LS	LS	LS	TOF	TOF	TOF	TOF
Integration Time	50μs	50μs	50μs	50μs	50μs	-	50μs	-
Well Capacity	40fF	53fF	40f	37fF	10fF	-	40fF	-
ADC/TDC	1bit	1-bit	1-bit	1-bit	1bit	90ns	1bit	90ns
Signal Light	46.8dB	43.9dB	43.5dB	43.5dB	23.6dB	29.8dB	43.5dB	20dB
Background Light	60.6dB	73.8dB	63.5	103.5	92dB	90.6dB	83.5	12dB
SBR’ Max	63.5dB	83.2dB	51dB	83dB	62.0dB	68dB	62dB	65dB
SBR’ Min	0.8dB	-56.5dB	0.06dB	-62dB	-34dB	-26dB	-62dB	40dB
Range Accuracy Max	1.21mm	3.38mm	1.2mm	1.5mm	27mm	50mm	12.6mm	5.8
Range Accuracy Min	0.37mm	1.5mm	0.4mm	0.6mm	6mm	9mm	40.7mm	37

Chapter 6

Conclusion

In this research, we have proposed method for the comprehensively evaluation of background light suppression characteristics and range finding accuracy for image sensors which is used for 3-D Measurement.

Four typical image sensors using light section method and time-of-flight method for 3-D measurement were taken as the base to analysis the background light suppression characteristics and issues which could affect the range finding accuracy in this work. We find out the evaluation method which can comprehensively evaluate the background light suppression characteristics and range finding accuracy for image sensors using for 3-D measurement.

Firstly, we evaluated the background light suppression characteristics and range finding accuracy of the high speed and high accurate image sensor with light-section method which has a conventional pixel circuit. By using our proposed method. The evaluation results of background light Suppression Characteristic shows this sensor has a 20.83dB SBR' while the signal is 0.01V, the background light is 0.001V and has a 0.06dB SBR' and while while the signal is 1.5V the background light is 0.24V, the voltage is proportional to signal light intensity and background light intensity respectively. The range of signal light intensity in some level of background light while the range information can be derived is successfully evaluated, the range of signal light intensity is 0.01V$\sim$1.5V, while the background light intensity is 0.001V. The range of background Intensity in some level of signal light while the range information can be derived is successfully evaluated. The range of background light is 0.001V$\sim$0.241V while signal light intensity is 1.5V. Range of background and signal Intensity while the range information can be derived is successfully evaluated. The range of background light intensity is 63.5dB, the range of signal light intensity range is 43.5dB. The evaluation results of range finding accuracy shows that the range accuracy with signal light intensity and background light Intensity is successfully evaluated 0.004 pixel pitch∼0.089 pixel pitch while the range of background light intensity is 63.5dB , the range of signal light intensity is 43.5dB.

Next we made a evaluation of the background light suppression characteristics and range finding accuracy of the high dynamic range and high background Light suppression image sensors with light-section Method.

The evaluation results of background light Suppression Characteristic shows range of signal light intensity in some level of background light while the range information can be derived is successfully evaluated. The range of background light intensity in some level of signal light while the range information can be derived is also successfully evaluated. And the range of background light and signal intensity while the range information can be derived is successfully evaluated. The range of background light intensity is 103.5dB, the range of signal light intensity range is 43.5dB. The gain of current mirror should be evaluated for the effect of SBR ’ is successfully evaluated. The evaluation results of range finding accuracy shows that range accuracy with signal light intensity and background light intensity is successfully evaluated. The accuracy is 0.004 pixel pitch∼0.089 pixel pitch in the same signal and background light condition. We found out the relation between range accuracy and numbers of averaging and this relation is successfully evaluated.

Then, the background light suppression characteristics and range finding accuracy of Time-of-Flight image sensor with lock-in pixel structure is evaluated by using the presented method.

The evaluation results of background light suppression characteristic shows: range of signal light intensity in some level of background light while the range information can be derived is successfully evaluated. And the range of background light Intensity in some level of signal light while the range information can be derived is successfully evaluated. Also the range of background light and signal Intensity while the range information can be derived is successfully evaluated. while the range of background light intensity is 103.5dB, the range of signal light intensity range is 43.5dB. The evaluation results of range finding accuracy shows the range accuracy with signal light intensity and background light intensity is successfully evaluated. The accuracy is 1.26 cm$\sim$4.07 cm And the relation of range accuracy with signal light intensity and background light intensity, numbers of averaging is successfully evaluated in the same signal and background light condition.

Lastly, the background light suppression characteristics and range finding accuracy of Time-of-Flight image sensor Single-Photon Avalanche Diodes is under analyzing and we will soon give the results.

As the final conclusions, we demonstrate methods which can realize the comprehensively evaluation of background light suppression characteristics which can successfully evaluated the range detectable area under the background light and signal light Range. and can also successfully evaluated the relation between background light,signal light,and SBR'. Meanwhile, We introduced the method to realize the comprehensively evaluation of range finding accuracy which can realize the successfully evaluated the range of accuracy under the background light and signal range and also can successfully evaluated the relation between background light,signal,and range accuracy. Using it we can even successfully evaluated the relation between background light,signal light ,and range accuracy and numbers of averaging.

These proposals will contribute to further evaluation of 3-D measurement using smart image sensors, we hope these method could help the researchers when they design the image sensors for 3-D measurement.

References

[1] Luo G., and Yang X., ”Fast Stereo Matching Algorithm Using Adaptive Window ”, Information Processing(ISIP), 2008 Int. Symp. 23-25 May 2008 pp.25-30.

[2] Ralf M.Philipp, and Ralph Etienne-Cummings, ”A 128 x 128 33mW 30frames/s Single Chip Stereo Imager ”, IEEE International Solid-State Circuit Conf.(ISSCC) Dig. Of Tech. Papers, 2006, pp.2050-2059.

[3] Gehrig S.K., and Franke U., ”Improving Stereo Sub-Pixel Accuracy for Long Range Stereo ”, in Proc of Int. Conf. on Computer Vision(ICCV) 2008, pp.1-7.

[4] Merrell P., Akbarzadeh A., Liang W., Mordohai P., Frahm J.-M., Ruigang Y., Nister D., and Pollefeys M., ”Real-Time Visibillity-Based Fusion of Depth Maps ”, in Proc of Int. Conf. on Computer Vision(ICCV) 2007, pp.1-8.

[5] H.Niitsuma, T Maruyama, “ Real-time generation of three-dimensional motion fields, ” International Conference on Field Programmable Logic and Applications, pp. 179-184, Aug. 2005.

[6] J.I.Woodfill, G.Gordon, R.Buck, “ Tyzx DeepSea High Speed Stereo Vision System, ” IEEE Computer Vision and Pattern Recognition(CVPR), 2004.

[7] K.Ambrosch, M.Humenberger, W.Kubinger,A.Steininger, “ Hardware implementation of an SAD based stereo vision algorithm ” IEEE Computer Vision and Pattern Recognition(CVPR), 2007.

[8] M.Hariyama, N.Yokoyama and M.Kameyama, “ 1000 frame/sec Stereo Matching VLSI Processor with Adaptive Window-Size Control ”, Proc. Asian Solid-State Circuits Conference (A-SSCC),pp.123-126, Nov. 2006.

[9] M.Hariyama, K.Tanji, and M.Kameyama, " FPGA Implementation of a High-Speed Stereo Matching Processor Based on Recursive Computation ", Proc. International Conference on Engineering of Reconfigurable Systems and Algorithms(ERSA), pp.263-266, 2009.

[10] C.Niclass, A.Rochas, P.-A.Besse, and E.Charbon, "Design and characterization of a CMOS 3-D image sensor based on single photon avalanche diodes ", IEEE J. Solid-State Circuit, vol.40, no.9, pp.1847-1854, Sept. 2005

[11] C.Niclass, C.Favi, T.Kluter, M.Gersbach, and E.Charbon, "A 128 × 128 Single-Photon Imager with on-Chip Column-Level 10b Time-to-Digital Converter Array ", IEEE Journal of Solid-State Circuits, Vol.43, no.12, pp.2977-2989, 2008.

[12] S.Kawahito, I.A.Halin, T.Ushinaga, T.Sawada, M.Homma, and Y.Maeda "A CMOS Time-of-Flight Rnage Image Sensor With Gates-on-Field-Oxide Structure " IEEE SENSOR Journal Vol.7, No.12, Dec. 2007.

[13] G.Yahav, G.J.Iddan, and D.Mandelboum," 3D imaging camera for gaming application, "in Proc. IEEE ICCE, Jan. 2007, pp.1-2.

[14] R.Jeremias, W.Brockherde, G.Doemens, B.Hosticka, L.Listl, P.Mengel, " A CMOS photosensor array for 3D imaging using pulsed laser, " IEEE International Solid-State Circuit Conf.(ISSCC) Dig. Of Tech. Papers, 2001, pp.252-253.

[15] R.Lange and P.Seitz," Solid-state time-of-Flight range camera, "IEEE J. Quantum Electron.,vol. 37, no. 3, pp. 390-397, Mar. 2001.

[16] R.Lange, " 3D Time-of-Flight distance measurement with custom solid-state image sensors in CMOS/CCD-technology ", Ph.D. Dissertation, University of Siegen, Germany, 2000.

[17] O.Elkhalili, O.M.Schrey, W.Ulfig, W.Brockherde, B.J.Hosticka, P. Mengel, L. Listl," A 64 × 8 Pixel 3-D CMOS Time Of Flight Image Sensor for Car Safety Applications, " in Proc. IEEE ESSCIRC, Sep. 2006.

[18] B.Saleh, M.Teich, " Fundamentals of Photonics ", ISBN 0-471-83965-5, John Wiley & Sons, 1991.

[19] K.Creath, " Phase-Measurement Interferometry Techniques ", Progress in Optics, Vol. 26, E. Wolf Ed., Elsevier, 1988.

[20] E.Hecht, A.Zajac, " OPTICS ", Addison-Wesley, 1974.

[21] E.Zimmermann et al., " Stabilized three-wavelength source calibrated by electronic means for high-accuracy absolute distance measurements ", Optics Letters, Vol. 21, pp. 531-533, 1996.

[22] R.Schwarte, " Principles of 3-D Imaging Techniques ", in Handbook of Computer Vision and Applications, B. Johne, H. Haussecker and P. Geissler (Eds.), Academic Press, 1999.

[23] K.Engelhardt, " Methoden und Systeme der optischen 3-D Messtechnik ", XI. Internationaler Kurs fur Ingenieurvermessung in Zurich, Ferd. Dummlers Verlag Bonn, 1992.

[24] S.Bourquin, " Low-coherence interferometry based on customized detector arrays ", Ph.D. Dissertation EPFL-Lausanne, Switzerland, No.2171, 2000.

[25] S.Yoshimura, T.Sugiyama, K.Yonemoto and K.Ueda, " A 48kframe/s CMOS Image Sensor for Real-time 3-D Sensing and Motion Detection ", IEEE International Solid-State Circuit Conf.(ISSCC) Dig. Of Tech. Papers, 2001, pp.94-436.

[26] Y.Oike, M.Ikeda, and K.Asada, " Design and Implementation of Real-Time 3-D Image Sensor With 640 x 480 Pixel Resolution ", IEEE J. Solid-State Circuit, vol.39, no.4, pp.622-628, April. 2004.

[27] Y.Oike, M.Ikeda, and K.Asada, " A 120 x 110 Position SensorWith the Capability of Sensitive and Selective Light Detection in Wide Dynamic Range for Robust Active Range Finding ", IEEE J. Solid-State Circuit, vol.39, no.1, pp.246-251, Jan. 2004.

[28] Y.Oike, M.Ikeda, and K.Asada,“ 640 x 480 Real-Time Range Finder Using High-Speed Readout Scheme and Column-Parallel Position Detector ”, IEEE Symp. VLSI Circuits Dig. Of Tech Papers, pp.153-156. 2003.

[29] Y.Oike, H. Shintaku, S. Takayama, M.Ikeda, and K.Asada, “ Real-Time and High-Resolution 3-D Imagein System Using Light-Section Method and Smart CMOS Sensor ”, in Proc. of IEEE Int. Conf. on Sensors (IEEE SENSORS), pp.502-507, 2003.

[30] T.Nezuka, M.Ikeda, and K.Asada, ”A Smart Position Sensor with Row Parallel Position Detection for High Speed 3-D Measurement, ” in Proc. of IEEE European Solid-State Circuits Conference (ESSCIRC), pp.101-105, Sep. 2002.

[31] Y.Oike, M.Ikeda, and K.Asada, ”A 375 x 365 High-Speed 3-D Range-Finding Image Sensor Using Row-Parallel Search Architecture and Multi-Sampling Technique, ” IEEE Journal of Solid-State Circuits, Vol.40, No.2, pp.444-453, Feb. 2005.

[32] J.Batlle, E.Mouaddib, J.Salvi, ”Recent progress in coded structured light as a technique to solve the correspondence problem : A Survey, ”Pattern Recognition, 31(7), pp.963-982, 1998.

[33] F.Chen, G.M.Brown, M.Song, ”Overview of three-dimensional shape measurement using optical methods, ” Optical Engineering, 39(1), pp.10-22, 2000.

[34] Jaehyuk Choi, Sang-Wook Han, Seong-Jin Kim, Sun-II Chang, and Euisik Yoon, ”A Spatial-Temporal Multi-Resolution CMOS Image Sensor with Adaptive Frame Rates for Moving Objects in the Region-of-Interest ”, IEEE Int. Solid-State Circuits Conf.(ISSCC) ISSCC Dig. of Tech. Papers, 2008, pp.502 - 503

[35] S.Mandai, T.Momma, T.Nakura, M.Ikeda, and K.Asada, ”Multi Functional Range Finder Employing a Dual Imager Core on a Single Chip ”, Int. SoC Design Conf. 2008, accepted.

[36] Y.Nitta, Y.Muramatsu, K.Amano, T.Toyama, J.Yamamoto, K.Mishina, A.Suzuki, T.Taura, A.Kato, M.Kikuchi, Y.Yasui, H.Nomura, and N.Fukushima, ”High-Speed Digital

Double Sampling with Analog CDS on Column Parallel ADC Architecture for Low-Noise Active Pixel Sensor ”, IEEE International Solid-State Circuit Conf.(ISSCC) Dig. Of Tech. Papers, 2006, pp.2024-2031.

[37] S.Mandai, T.Nakura, M.Ikeda, and K.Asada, “ Ultra High Speed 3-D Image Sensor ”, International Image Sensor Workshop(IISW), Jun. 2009.

[38] S.Mandai, M.Ikeda, and K.Asada, “ A 256 × 256 14k Range Maps/s 3-D Range-Finding Image Sensor Using Row-Parallel Embedded Binary Search Tree and Address Encoder, ” IEEE International Solid-State Circuits Conference(ISSCC), Dig. Of Tech. Papers, pp.404-405, Feb. 2010.

[39] C.Niclass, C.Favi, T.Kluter, M.Gersbach, and E.Charbon, ”A 128x128 Single-Photon Imager with on-Chip Column-Level 10b Time-to-Digital Converter Array Capable of 97psResolution ”, IEEE International Solid-State Circuit Conf.(ISSCC) Dig. Of Tech. Papers, 2008, pp.44-594.

[40] R.B.Staszewski, S.Vemulapalli, P.Vallur, J.Wallberg and P.T.Balsara, ”1.3 V 20 ps time-to-digital converter for Frequency Synthesis in 90-nm CMOS ” IEEE Trans. on Circuits and Systems II, vol. 53, no. 3, pp.220-224, Mar. 2006.

[41] Y.Arai and T.Baba, ”A CMOS time to digital converter VLSI for high energy physics ” IEEE Symp. VLSI Circuits Dig. Of Tech Papers, 1988, pp.121-122.

[42] P.Dudek, S.Szczepanski, and J.V.Hatfield, ”A High-Resolution CMOS Time-to-Digital Converter Utilizing a Vernier Delay Line ”, IEEE Trans. on Solid-State Circuits, Vol.35,No.2, Feb. 2000, pp.240-247.

[43] P.Chen, S.I.Liu, and J.Wu, ”A CMOS Pulse-Shrinking Delay Element For Time Interval Measurement ”, IEEE Trans. on Circuits and Systems-II Analog and Digital Signal Processing, Vol.47, No.9, Sep 2000, pp.954-958.

[44] J.P.Jansson, A.Mantyniemi, and J.Kostamozaara, ”A CMOS Time-to-Digital Converter With Better Than 10 ps Single-Shot Precision ”, IEEE Journal of Solid-State Circuits,Vol.41, No.6, June 2006, pp.1286-1296.

[45] B.M.Helal, M.Z.Straayer, G.Y.Wen, and M.H.Perrott, ”A Low Jitter 1.6GHz Multiplying DLL Utilizing a Scrambling Time-to-Digital Converter and Digital Correlation ”, IEEE Symp. VLSI Circuits Dig. Of Tech Papers, 2007, pp.156-157.

[46] A.Mantyniemi and T.Rhkone, and J.Kistamovaara, ”A CMOS Time-to-Digital Converter Based On a Cyclic Time Domain Successive Approximation Interpolation Method ” IEEE Journal of Solid-State Circuits, Vol.44, No.11,Nov. 2009.

[47] S.Henzler, S.Koeppe, W.Kamp, H.Mulatz, and Doris.S.L, ”90nm 4.7ps-Resolution 0.7-LSB Single-Shot precision and 19pJ-per-Shot Local Passive Interpolation Time-to-Digital Converter with On-Chip Characterization ”, IEEE International Solid-State Circuit Conf.(ISSCC) Dig. Of Tech. Papers, 2008, pp.548-635.

[48] Minjae Lee and Asad A. Abidi, ”A9b,1.25ps Resolution Coarse-Fine Time-to-Digital Converter in 90nm CMOS that Amplifies a Time Residue ” IEEE Journal of Solid-State Circuits,Vol.43, No.4,Apr. 2008.

[49] T.Nakura, S.Mandai, M.Ikeda and K.Asada, ”Time Difference Amplifier using Closed-Loop Gain Control ”, IEEE Symp. VLSI Circuits Dig. of Tech Papers, pp.208-209, Jun. 2009.

[50] S.Mandai, T.Nakura, M.Ikeda and K.Asada, ”Cascaded Time Difference Amplifier using Differential Logic Delay Cell ”, ISOCC, pp.194-197, Nov. 2009.

[51] S.Mandai, T.Nakura, M.Ikeda, and K.Asada, “ A 8bit Two Stage Time-to-Digital Converter Using 16x Cascaded Time Difference Amplifier in 0.18um CMOS, ”in Proceedings of IEEE Mediterranean Electrotechnical Conference(MELECON), to be presented, Apr. 2010.

[52] E. Charbon, " Will CMOS Imagers Ever Need Ultra-High Speed? ", IEEE International Conference on Solid-State and Integrated-Circuit Technology, 1975-1980 (2004).

[53] S. Cova, A. Longoni, and A. Andreoni, " Towards Picosecond Resolution with Single-Photon Avalanche Diodes ", Rev. Sci. Instr., 52(3), 408-412 (1981).

[54] R.J. McIntyre, " Recent Developments in Silicon Avalanche Photodiodes ", Measurement, 3(4), 146-152 (1985).

[55] A. Spinelli and A. L. Lacaita, " Physics and Numerical Simulation of Single Photon Avalanche Diodes ", IEEE Trans. on Electron Devices, 44(11), 1931-1943 (1997).

[56] A. Rochas et al., " Single Photon Detector Fabricated in a Complementary Metal Oxide Semiconductor High voltage Technology ", Rev. Sci. Instr., 74(7), 3263-3270 (2003).

[57] E. Charbon, " Single-photon Imaging in CMOS " Proc. of SPIE Vol. 7780 77801D-15.

[58] Y.OYIKE, " Smart Image Sensors and Associative Engines for Three Dimensional Image Capture ", Ph.D. Dissertation, University of Tokyo, Japan, 2004.

[59] Y.Yachide, " Real-Time 3-D Measurement System Based on Light-Section Method Using Smart Image Sensor ", ICIP, 2005.

[60] J.Cheon, " Smart CMOS Image Sensor With High SBR and Subpixel Resolution for Light-Section-Based Range Finding ", IEEE Electron Devices Society, 2009.

[61] D. Stoppa, L. Viarani, A. Simoni, L. Gonzo, M. Malfatti, and G. Pedretti, " A 16 × 16-pixel range-finding CMOS image sensor, " in Proc. ESSCIRC, Leuven, Belgium, Sep. 2004, pp. 419-422.

[62] G.Zach, " A 16 x 16 Pixel Distance Sensor With In-Pixel Circuitry That Tolerates 150klx of Ambient Light ", JSSC, vol.45. No.7.2010

謝辞

本論文は多くの方々のご指導やご協力・支えがあって完成することができました。ここに記して深く感謝しお礼を申し上げます。

とりわけ、東京大学大学院の池田誠准教授からは指導教官として、厳しくも暖かいご指導を頂きました。本論文は、今から考えると学問的な厳密さを追求するにはやや難しいテーマだったようで、何度も壁に突き当たっては挫けそうになった 2 年間を、池田先生は激励しつつ辛抱強くご指導をくださいました。

その間、同大学院の浅田邦博教授、名倉徹准教授、飯塚哲也講師には、それぞれのご専門のお立場からさまざまな貴重なご助言、ご指導をいただき、また良好な研究環境を与えて下さり心より感謝申し上げます。

修士課程在学中、同期の神谷歩未氏、吉川俊之氏、中里輝希氏の存在が研究を進めていく上で、大きな励みとなったことをここに記すともに、心より感謝申しあげます。

研究活動においてのみでなく、他の様々な場面においても常に議論を共にして頂き、多くの貴重なご意見を頂いた研究員の Tse-Wei Chen 博士及び大学院生の門馬太平氏、Bushnaq Sanad Saleh 氏、Devlin Benjamin Stefan 氏に深く感謝致します。

日頃から研究活動を共にし、多くの助言を頂いた大学院生の齊藤総氏、王楠氏、児玉和俊氏、矢部紘貴氏、久保田透氏、卒論生の宮崎耕太郎氏、西部拓人氏、中村陽二氏、研究生の Parit Kanjanavirojkul 氏に深く感謝致します。

さまざまな場で数多くのご助言、ご支援を下さいました OB の Nguyen Ngoc Mai Khanh 博士、金鎮明博士、萬代新悟氏（TU Delft）、服部慶士氏（グーグル（株））、程在鉉（LG(株)）、玉置裕基氏（任天堂（株））、宋暁旭氏（ゴールドマン・サックス（株））、秘書の横地順子氏、山中知歩氏に深く感謝致します。

最後に，いつも心の支えになってくれた中国に住む両親と外祖母に心から感謝します。そして、どのような状況においても応援してくれた素晴らしい妻の陳明シュ、娘の胡梓キに精一杯の感謝を捧げます。